












A rust-fungus Nudix hydrolase effector decaps mRNA *in vitro* and interferes with plant immune pathways

Carl L. McCombe^{1*} , Ann-Maree Catanzariti^{1*} , Julian R. Greenwood¹ , Anna M. Desai², Megan A. Outram¹ , Daniel S. Yu¹ , Daniel J. Ericsson³ , Steven E. Brenner² , Peter N. Dodds⁴ , Bostjan Kobe⁵ , David A. Jones¹  and Simon J. Williams¹ 

¹Plant Sciences Division, Research School of Biology, The Australian National University, Canberra, ACT 2601, Australia; ²Plant and Microbial Biology Department, University of California, Berkeley, CA 94720, USA; ³Australian Synchrotron, Macromolecular Crystallography, Clayton, Vic. 3168, Australia; ⁴Black Mountain Science and Innovation Park, CSIRO Agriculture and Food, Canberra, ACT 2601, Australia; ⁵School of Chemistry and Molecular Biosciences, Institute for Molecular Bioscience and Australian Infectious Diseases Research Centre, University of Queensland, Brisbane, Qld 4072, Australia

Summary

- To infect plants, pathogenic fungi secrete small proteins called effectors. Here, we describe the catalytic activity and potential virulence function of the Nudix hydrolase effector AvrM14 from the flax rust fungus (*Melampsora lini*).
- We completed extensive *in vitro* assays to characterise the enzymatic activity of the AvrM14 effector. Additionally, we used *in planta* transient expression of wild-type and catalytically dead AvrM14 versions followed by biochemical assays, phenotypic analysis and RNA sequencing to unravel how the catalytic activity of AvrM14 impacts plant immunity.
- AvrM14 is an extremely selective enzyme capable of removing the protective 5' cap from mRNA transcripts *in vitro*. Homodimerisation of AvrM14 promoted biologically relevant mRNA cap cleavage *in vitro* and this activity was conserved in related effectors from other *Melampsora* spp. *In planta* expression of wild-type AvrM14, but not the catalytically dead version, suppressed immune-related reactive oxygen species production, altered the abundance of some circadian-rhythm-associated mRNA transcripts and reduced the hypersensitive cell-death response triggered by the flax disease resistance protein M1.
- To date, the decapping of host mRNA as a virulence strategy has not been described beyond viruses. Our results indicate that some fungal pathogens produce Nudix hydrolase effectors with *in vitro* mRNA-decapping activity capable of interfering with plant immunity.

Authors for correspondence:

Simon J. Williams

Email: simon.williams@anu.edu.au

David A. Jones

Email: david.jones@anu.edu.au

Received: 20 September 2022

Accepted: 2 January 2023

New Phytologist (2023)

doi: 10.1111/nph.18727

Key words: AvrM14, fungal effectors, *Melampsora lini*, mRNA decapping, Nudix hydrolase, plant immunity.

Introduction

Infectious diseases represent a significant threat to global crop production. To facilitate and maintain infection, plant pathogens secrete an array of proteins (termed effectors; Lo Presti *et al.*, 2015). Effectors are either delivered to the apoplast or translocated inside host cells, to modulate cellular processes. Plants have evolved resistance genes (*R*-genes) to defend against pathogen infection. Resistance genes encode effector-detecting resistance proteins (R-proteins) capable of inducing a strong immune response, known as effector-triggered immunity (ETI; Jones & Dangl, 2006; Dodds & Rathjen, 2010). The activation of ETI typically prevents pathogen growth, and recognised effectors are therefore referred to as avirulence (Avr) proteins. The ability of effectors to promote infection while avoiding recognition is crucial for successful infection. Consequently, understanding the pathogenicity function of effectors and how they are

perceived by R-proteins remains a major focus in the study of plant–pathogen interactions.

Nucleoside diphosphate linked to moiety-X (Nudix) hydrolase domains have been predicted in effectors from multiple fungal, oomycete and bacterial plant pathogens (Dong & Wang, 2016). The putative Nudix hydrolase effectors were identified based on similarities with the Nudix-box consensus sequence (GX₅EX₇-REUXEEXGU, where *U* is usually a hydrophobic residue and *X* is any amino acid). Nudix hydrolases typically hydrolyse nucleoside diphosphates bound to an additional moiety and substrate specificity is generally controlled by residues outside the Nudix box (McLennan, 2006; Srouji *et al.*, 2017). Well-characterised substrates of Nudix hydrolases include nucleoside triphosphates (Sakumi *et al.*, 1993; Ito *et al.*, 2005; Jemth *et al.*, 2018), adenosine diphosphate ribose (ADPR) (O'Handley *et al.*, 1998; Gabelli *et al.*, 2002; Kang *et al.*, 2003; Perraud *et al.*, 2003), diadenosine polyphosphates (ApnAs; Bessman *et al.*, 2001; Leslie *et al.*, 2002; Iwai *et al.*, 2004) and the 5' cap of mRNA transcripts (Van Dijk

*These authors contributed equally to this work.

et al., 2002; Wang *et al.*, 2002; Song *et al.*, 2013). Nudix hydrolases are ubiquitous in prokaryotic and eukaryotic organisms and are involved in diverse physiological processes and cellular homeostasis (McLennan, 2006).

The first Nudix hydrolase effector to be experimentally validated was Avr3b from the oomycete *Phytophthora sojae*, a destructive pathogen of soybean. Transient expression of Avr3b in *Nicotiana benthamiana* increased susceptibility to *Phytophthora capsica* and *Phytophthora parasitica* infection, diminished reactive oxygen species (ROS) accumulation around invasion sites, and reduced plant cell death during infection (Dong *et al.*, 2011). In soybean, the expression of Avr3b suppressed cell death triggered by the recognition of Avr1b (Dong *et al.*, 2011). Avr3b requires a plant cyclophilin for enzymatic activation, and both the cyclophilin and the Nudix box are required for the identified Avr3b virulence activities (Dong *et al.*, 2011; Kong *et al.*, 2015). Avr3b hydrolyses multiple nucleoside diphosphate compounds *in vitro* (Dong *et al.*, 2011). Recently, Yu *et al.* (2022) demonstrated that Avr3b also has phosphodiesterase activity against 2',3'-cAMP/GMP and suggest that this enzymatic activity is a virulence function of the effector (Yu *et al.*, 2022). The promiscuous *in vitro* enzymatic activity of Avr3b is common among Nudix hydrolases (McLennan, 2013) and complicates the identification of the true substrates of the effector during infection. RipN, a Nudix hydrolase effector from the bacterial pathogen *Ralstonia solanacearum*, also hydrolyses a variety of nucleoside diphosphate substrates *in vitro* (Sun *et al.*, 2019). The preferred *in vitro* substrates of RipN are NADH and ADPR; however, overexpression of RipN in *Arabidopsis thaliana* did not result in significant changes to ADPR, NAD⁺ or NADH levels (Sun *et al.*, 2019). CtNUDIX, a putative Nudix hydrolase effector from the hemibiotrophic fungus *Colletotrichum truncatum*, elicits a cell-death response when transiently expressed in *Nicotiana tabacum* (Bhadauria *et al.*, 2013). However, it is unknown whether CtNUDIX possesses hydrolase activity and what it targets during infection. Putative Nudix hydrolase effectors have also been identified in biotrophic fungal pathogens. The flax rust-fungus *Melampsora lini* expresses *AvrM14* early in infection of flax, *AvrM14* encodes a predicted Nudix hydrolase effector (Anderson *et al.*, 2016; Wu *et al.*, 2019). The AvrM14 effector is recognised by the flax immune receptors M1 and M4, with previous research on AvrM14 immune recognition indicating that the effector is translocated inside flax cells during infection (Anderson *et al.*, 2016). Here, we report the structure, biochemical activity and likely virulence function of the AvrM14 protein.

Materials and Methods

Cloning

AvrM14-A and AvrM14-B, without the predicted signal sequence (residues 22–166), were PCR-amplified from *Melampsora lini* cDNA (primers listed in Supporting Information Table S1) to facilitate respective downstream cloning processes.

AvrM14 mutants were generated using the Phusion Site-Directed Mutagenesis Kit (Thermo Fisher Scientific, Waltham, MA, USA) and 5' phosphorylated primers (Table S1).

For transient expression of AvrM14 *in planta*, T-DNA plasmids were generated using Gateway cloning. The constructs were initially cloned into the pENTR/D-TOPO entry vector and then into the pEarleyGate (pEG) destination vectors pEG102 or pEG104 (Earley *et al.*, 2006). All constructs were cloned with 3' stop codons after the coding sequence, resulting in the expression of untagged (pEG102) or N-terminal YFP-tagged (pEG104) proteins *in planta*. The M1 sequence was cloned into the pTN35S plant expression vector (Dodds *et al.*, 2004).

For recombinant protein production in *Escherichia coli*, the AvrM14-A, AvrM14-B, AvrM14-A^{E82Q} and AvrM14-B^{E82Q} sequences were cloned into the pMCSG7 vector using ligation-independent cloning (Stols *et al.*, 2002). The resulting plasmids encoded an N-terminal hexahistidine (6×His) tag, followed by a tobacco etch virus protease cleavage site allowing 6×His tag removal. AvrM14 homologues from other *Melampsora* spp. were ordered as *E. coli* codon-optimised double-stranded DNA fragments without the predicted signal sequences from Integrated DNA Technologies Inc. (IDT[®], Coralville, IA, USA). The DNA fragments were cloned into a modified pOPIN vector (Bentham *et al.*, 2021), resulting in an N-terminal 6×His tagged construct with a 3C protease site in-between the 6×His-tag and the coding sequence for each homologue. All protein sequences following purification and tag-cleavage are listed in Table S1.

Protein production

Recombinant HsNudt16 protein was purchased from Abcam (Cambridge, UK). All other proteins were expressed in *E. coli* BL21 (DE3) cells and purified using nickel metal affinity chromatography, followed by size-exclusion chromatography. For full details of protein production, see Methods S1.

Crystallisation and structure determination

Initial crystallisation screening with purified AvrM14-A and AvrM14-B monomeric proteins was conducted using a Mosquito robot (STP LabTech, Melbourn, UK) in a 96-well plate format using sparse matrix screens. The hanging drop vapour-diffusion method of crystallisation was used and drops consisting of 100 nl 10 mg ml⁻¹ protein solution and 100 nl reservoir solution were equilibrated against 100 µl reservoir solution. The final optimised condition for monomeric AvrM14-A (10 mg ml⁻¹) was 2.4 M sodium malonate pH 6.0 and 2% glycerol. For monomeric and homodimeric AvrM14-B, the condition utilised for crystallisation was 1.8 M (NH₄)₂SO₄, 100 mM sodium acetate (pH 4.33) and 100 mM MgCl₂.

Before X-ray data collection, AvrM14-A crystals were transferred to 2.4 M sodium malonate pH 6.0 and 10% glycerol, before flash-cooling in liquid nitrogen. To enable phasing, some AvrM14-A crystals were soaked in a solution of 2.4 M sodium malonate pH 6.0, 10% glycerol and 1 M NaBr. AvrM14-B

crystals were transferred to the same condition used for crystallisation supplemented with 20% glycerol, before flash-cooling in liquid nitrogen.

Single-wavelength anomalous diffraction (SAD) and native datasets were collected on the MX1 and MX2 beamlines at the Australian Synchrotron (Table S2; Cowieson *et al.*, 2015; Aragão *et al.*, 2018). The datasets were processed in XDS (Kabsch, 2010) and scaled using AIMLESS in the CCP4 suite (Evans & Murshudov, 2013). For SAD phasing of AvrM14-A, the CRANK2 pipeline (Skubák & Pannu, 2013) was used in the CCP4 suite. The best chain from the autobuilt model was then used as a search model to solve the structure of a native dataset using maximum-likelihood molecular replacement (MR) with Phaser in Phenix (Liebschner *et al.*, 2019).

The crystal structure of monomeric and homodimeric AvrM14-B was determined using maximum-likelihood MR with Phaser in Phenix (Liebschner *et al.*, 2019). The MR search model was chain A of the AvrM14-A crystal structure. For all native datasets, automated model building and initial refinement were completed using either Phenix AutoBuild (Terwilliger *et al.*, 2008) or ARP/wARP (Langer *et al.*, 2008). Subsequent model building was carried out manually in Coot (Casañal *et al.*, 2020) in-between rounds of automated refinement using Phenix refine (Afonine *et al.*, 2012). MolProbity was used for validation of the final models (Williams *et al.*, 2018). Analysis of the final structures was performed with COOT (Casañal *et al.*, 2020), PyMOL, APBS (Jurrus *et al.*, 2018) and ESPRIT v.3.0 (Robert & Gouet, 2014).

Map coordinates and structure files have been deposited in the Protein Data Bank (AvrM14-A Monomer: 8DP8, AvrM14-B Monomer: 8DP9, AvrM14-B Homodimer: 8DPA).

Nudix hydrolase substrate screening assays

To assess phosphohydrolase activity against ADPR, NADH, Ap₄A, FAD and NAD⁺, 6 µM of recombinant protein was incubated with 2 mM substrate in a reaction buffer containing 50 mM Tris-HCl pH 8.5, 5 mM MgCl₂, 1 mM DTT and 40 U ml⁻¹ of alkaline phosphatase at 37°C for 30 min. To detect inorganic phosphate produced from the reactions, a phosphomolybdate method was used (Ames, 1966). Sulphuric acid was added to a final concentration of 500 mM; ammonium molybdate was added to a final concentration of 2 mM and ascorbic acid to a final concentration of 60 mM; the solution was then incubated at 45°C for 10 min, and the absorbance at 820 nm was recorded.

A kinetic screening method with a phosphate sensing fluorophore (Nguyen *et al.*, 2016) was used to measure phosphohydrolase activity against 69 unique nucleoside diphosphates (substrates and their groups are listed in Table S3). In short, the standard reaction contained 10 mM Tris-HCl pH 7.6, 1 mM MgCl₂, 5 µM phosphate sensor (Thermo Fisher Scientific), 0.05 U ml⁻¹ of yeast pyrophosphatase (PPase) when pyrophosphate was a predicted product or 1 U ml⁻¹ of alkaline phosphatase (APase) when a nucleoside monophosphate was a predicted product. Each substrate concentration was 5 µM in both grouped and ungrouped reactions. AvrM14-A recombinant protein concentration was 50 nM. The

mixtures were incubated at 37°C and monitored continuously for 30 min on a Tecan GENios Microplate Reader with the following parameters: λ-excitation = 425 nm, λ-emission = 465 nm, gain 60, 100 cycles, 37°C.

The subsequent kinetic screen to assess AvrM14-A, AvrM14-B, AvrM14-A^{E82Q} and AvrM14-B^{E82Q} hydrolase activity against ^{m7}Gp₅G (Jena Bioscience, Jena, Germany) was completed as above, with some modifications to optimise activity. The reaction mixture contained 10 mM Tris-HCl (pH 7.6), 2 mM MnCl₂, 1 U ml⁻¹ alkaline phosphatase, 5 µM ^{m7}Gp₅G, 2.5 µM phosphate sensor (Thermo Fisher Scientific) and 100 nM purified recombinant protein in a total volume of 100 µl. Fluorescence measurements (excitation at 425 nm and emission at 465 nm) were recorded every 10 s for 30 min using a Tecan Infinite® M1000 (Tecan, Männedorf, Switzerland) plate reader at room temperature.

RNA synthesis, purification, capping and decapping

A 231-nt synthetic RNA sequence (sequence in Table S1) was synthesised using the HiScribe™ T7 High Yield RNA Synthesis Kit (NEB, Ipswich, MA, USA) following the recommended protocol. The RNA was purified using RNeasy Clean XP beads (Beckman Coulter, Brea, CA, USA). Purified RNA was capped using the Vaccinia Capping System (NEB) with GTP spiked with (α-³²P)-GTP (PerkinElmer, Waltham, MA, USA). To purify the capped RNA, the Monarch® RNA Cleanup Kit (NEB) was used, and two purifications were completed per capping reaction to ensure near-complete removal of (α-³²P)-GTP.

RNA-decapping assays were completed as described previously, with some minor modifications (Song *et al.*, 2013). In brief, 2 µM recombinant protein was incubated with capped RNA in a reaction buffer with 10 mM HEPES (pH 7.5), 150 mM NaCl, 2 mM MnCl₂, 1 mM DTT and 40 U ml⁻¹ RNase Inhibitor (Merck, Rahway, NJ, USA) for 30 min at 37°C. The reaction products were separated using PEI-cellulose TLC plates (Merck) with 0.45 M (NH₄)₂SO₄ as the liquid phase. Dried plates were placed into a cassette with a K-screen (Bio-Rad) and left for 14–18 h before imaging using a PharosFX™ scanner (Bio-Rad). To identify the reaction products, known standards of ^{m7}GMP (Jena Bioscience), ^{m7}GDP (Jena Bioscience), GMP (Merck) and GDP (Merck) were separated using the same TLC conditions and imaged using UV shadowing.

Plant materials and growth conditions

Nicotiana benthamiana and *N. tabacum* L. plants were grown in soil in a controlled environment at 25°C with a 16-h day length. Flax (*Linum usitatissimum* L.) plants were grown in soil in glasshouses with natural light at a constant temperature of 24°C. Infiltration experiments were completed on 4–5-wk-old *N. benthamiana*, c. 7-wk-old *N. tabacum* and c. 3-wk-old *L. usitatissimum*.

Agroinfiltrations

Agroinfiltrations were completed as described previously (Catanzariti *et al.*, 2015). In brief, *Agrobacterium* strain GV3101

(pMP90) containing the pEG102, pEG104 or pTN35S DNA constructs (see 'Cloning' in the Materials and Methods section) were suspended in infiltration buffer (10 mM MES pH 5.6, 10 mM MgCl₂ and 200 μ M acetosyringone) to a final optical density at 600 nm of 1.0. All cultures were incubated in the dark at room temperature for 2 h before syringe-infiltration into either *N. benthamiana*, *N. tabacum* or *L. usitatissimum* leaves. Infiltrated plants were kept in the same growing conditions as before infiltration.

ROS burst assays

Measurement of ROS was completed as described previously with some minor modifications (Heese *et al.*, 2007). In brief, *N. benthamiana* leaf discs (4 mm diameter) were floated on water overnight in a 96-well plate. The water was replaced with an elicitor solution (100 μ M luminol, 10 μ g ml⁻¹ horseradish peroxidase and 100 nM flg-22 or 5 μ g ml⁻¹ chitin), and luminescence was measured over time using a Tecan Infinite® M1000 Pro (Tecan) plate reader at room temperature.

Immunoblot analysis

Rabbit polyclonal antibodies against recombinant AvrM14-A protein were produced and affinity purified by the Walter & Eliza Hall Institute of Medical Research (WEHI, Melbourne, Vic., Australia). Protein extraction from plant tissue for Western blotting was performed as described previously (108). Blots were probed with either rabbit anti-AvrM14 (pEG102 constructs) or mouse anti-GFP (pEG104 constructs; Roche) and detected by goat anti-rabbit-HRP (Merck) or goat anti-mouse-HRP (Cytiva, Marlborough, MA, USA). Clarity™ Western ECL substrate (Bio-Rad) was added to the immunoblots and chemiluminescence detected using a ChemiDoc imager (Bio-Rad).

SEC-MALS analysis

SEC-MALS was performed as described previously (Casey *et al.*, 2016). In brief, the purified protein samples were loaded onto a Superdex 75 Increase 10/300 size-exclusion column (Cytiva) pre-equilibrated in buffer (10 mM HEPES pH 7.5, 150 mM NaCl), connected to a Dawn Heleos II 18-angle light-scattering detector and an Optilab rEX refractive index detector (Wyatt Technology, Santa Barbara, CA, USA). The molecular masses of the proteins were calculated using ASTRA 6.1 software (Wyatt Technology).

RNA extractions, sequencing and analysis

Twenty flax leaves from a single plant (per replicate, with a total of four replicates for both the AvrM14-A and AvrM14-A^{E82Q} treatments and three replicates for the vector-only treatment) were collected 3 d postinfiltration with either the pEG102 AvrM14-A, pEG102 AvrM14-A^{E82Q} or empty vector (pEG102) GV3101 *Agrobacterium* constructs. Each replicate (20 leaves) was placed into a plastic tube with stainless steel beads and frozen in

liquid nitrogen. Plant tissue was lysed using the TissueLyser II (Qiagen). TRIzol™ reagent and the PureLink™ RNA Mini Kit (Thermo Fisher Scientific) were used for RNA purification from the lysed sample following the manufacturer's protocol.

Whole transcriptome RNA sequencing was conducted by Novogene (Beijing, China) using the Ribo-Zero Magnetic Kit (Illumina, San Diego, CA, USA) for rRNA depletion, random hexamers for cDNA synthesis, the NEBNext® Ultra™ Directional RNA Library Prep Kit (NEB) for library preparation and the Illumina Novaseq 6000 platform for sequencing. Raw sequencing data is available from the NCBI (GEO: GSE207874, SRA: SRX16112399, SRX16112400, SRX16112401, SRX16112402, SRX16112403, SRX16112404, SRX16112405, SRX16112406, SRX16112384, SRX16112385 and SRX16112386). For full details of RNA-Seq data analysis, see Methods S1.

Results

AvrM14 is an active Nudix hydrolase capable of interfering with plant immune responses

The AvrM14 effector from flax rust contains 146 amino acids as a mature protein that includes a Nudix-box consensus sequence (Anderson *et al.*, 2016). Two allelic variants of AvrM14 have been identified (AvrM14-A and AvrM14-B). AvrM14-A is recognised by flax R-proteins M1 and M4, while AvrM14-B possesses six amino acid polymorphisms and has escaped recognition (Anderson *et al.*, 2016). To understand the virulence function(s) of AvrM14 and how the AvrM14-B effector escapes recognition by M1 and M4, we determined the crystal structures of AvrM14-A and AvrM14-B at a resolution of 2.3 and 1.8 Å, respectively (see Table S2 for data collection and refinement statistics; the higher-resolution structure of AvrM14-B will be used for structure analyses unless indicated otherwise). The structures revealed that AvrM14 proteins display a characteristic Nudix-fold architecture, consisting of a β -grasp fold surrounding an α -helix (Fig. 1a; Lin *et al.*, 1997; Gabelli *et al.*, 2001). In typical Nudix hydrolases, the Nudix box folds into a loop- α -helix-loop structure, but for AvrM14, a 3_{10} -helix is present before the α -helix (Figs 1a, S1a). The 3_{10} -helix appears to compensate for the double amino acid insertion in the AvrM14 Nudix box (Anderson *et al.*, 2016), allowing the protein to maintain a salt bridge between a conserved Nudix-box glutamate (E71) and arginine (R81) found in canonical Nudix hydrolase structures (Fig. S1a; Gabelli *et al.*, 2001; Xu *et al.*, 2004). Nudix hydrolases require divalent metal ions for catalysis (Mildvan *et al.*, 2005; McLennan, 2006). While Mg²⁺ cations were included in our crystallisation solution for AvrM14-B, we did not observe clear density to suggest metal ion binding in the structures. Despite this, two of the three Nudix-box glutamate residues typically required for divalent metal binding (E85 and E86) are positioned in a similar location to previously determined metal-bound Nudix hydrolase structures (Fig. S1c; Gabelli *et al.*, 2002). The third Nudix-box glutamate, also often implicated in metal binding (E82), has dual conformations in our crystal structures. In one conformation, the side chain is buried under a β -sheet, whereas in the other, it is solvent-exposed (Fig. S1c). Based on previously determined metal-bound

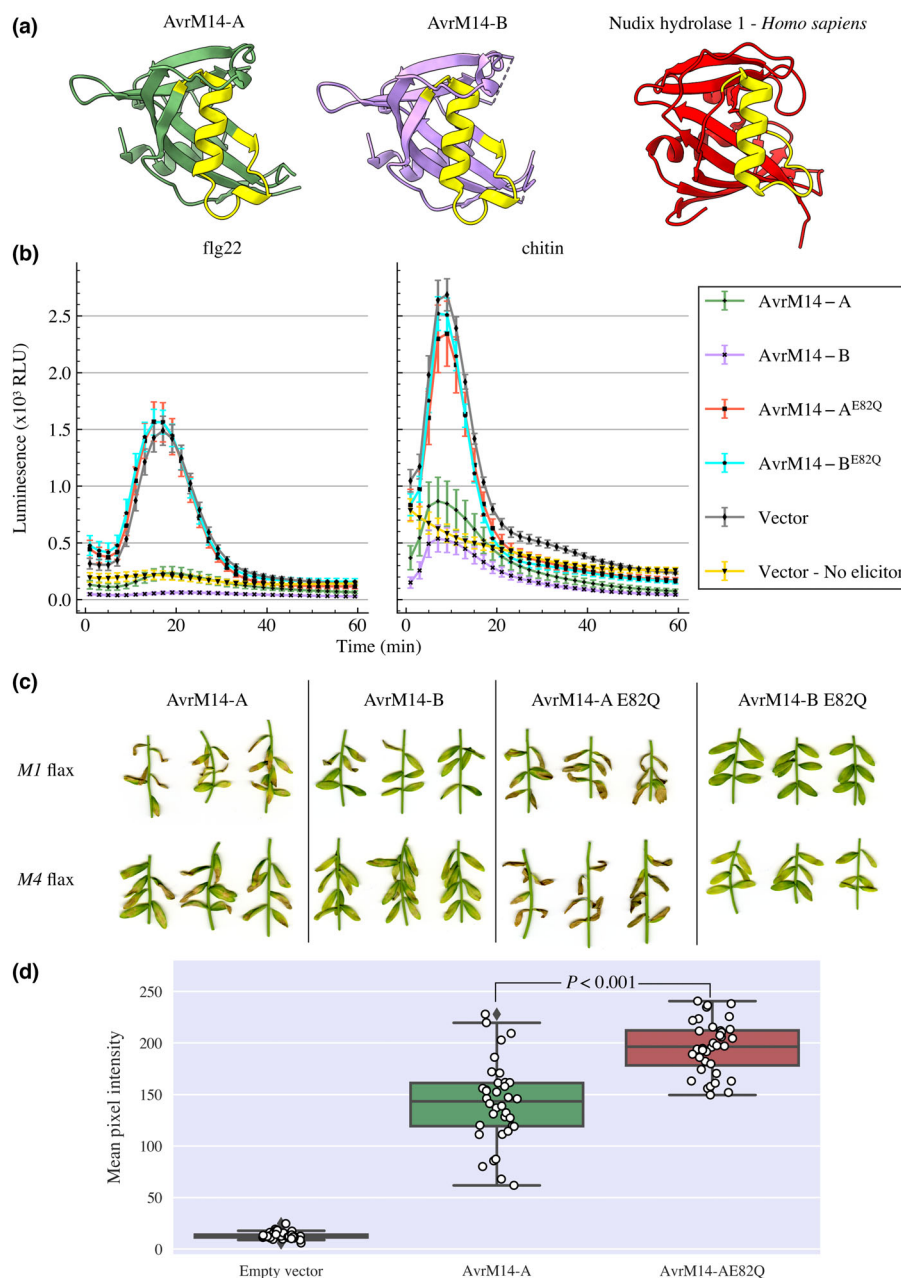


Fig. 1 Enzymatic activity of AvrM14, a Nudix hydrolase, suppresses reactive oxygen species (ROS) production, triggered by flg22 or chitin, and the hypersensitive response, triggered by the M1 resistance protein. (a) Ribbon diagrams of the AvrM14-A and AvrM14-B crystal structures, (PDB ID: 8DP8 and 8DP9) showing they adopt a Nudix fold. The Nudix-box region that typically folds into a loop- α -helix-loop is coloured yellow. For comparison to a prototypical Nudix hydrolase, the structure of Nudix hydrolase 1 (MTH1) from *Homo sapiens* is shown on the right (PDB ID: 5GHI) in analogous orientation (Waz *et al.*, 2017). (b) *Nicotiana benthamiana* leaves were infiltrated with *Agrobacterium* (GV3101) harbouring either an empty vector (pEG104) or pEG104 constructs encoding AvrM14-A, AvrM14-B, AvrM14-A^{E82Q} or AvrM14-B^{E82Q} proteins with YFP N-terminal tags expressed under the 35 S promoter from the cauliflower mosaic virus. At 4 days post-infiltration (dpi), leaf tissue was exposed to 100 nM flg-22 or 1 $\mu\text{g ml}^{-1}$ chitin (except in the no-elicitor treatment) and ROS production was recorded as relative luminescence units over time. Results are means \pm SEs ($n = 12$). (c) Bison \times M1 (Williston Brown) or M4 (Victory 'A') flax lines were agroinfiltrated to transiently express either wild-type or mutant AvrM14 proteins (AvrM14-A, AvrM14-B, AvrM14-A^{E82Q} and AvrM14-B^{E82Q}). Multiple leaves from three independent plants were infiltrated with each construct. The agroinfiltrated leaves were photographed 7 dpi. (d) Bison \times M1 (Williston Brown) flax leaves were agroinfiltrated with an empty vector or with constructs to transiently express either wild-type or mutant AvrM14-A proteins (AvrM14-A and AvrM14-A^{E82Q}). At 6 dpi, all infiltrated leaves were collected and the cell-death response for each leaf was assessed by pixel intensity analysis using IMAGEJ after imaging the leaves with a Chemidoc MP imager. There were 36 replicates for each treatment, as indicated by the white dots on top overlaying the boxplots. In the boxplots the horizontal line in the middle of the box represents the median value, the box represents the interquartile range (IQR), the whiskers extend to 1.5 \times IQR, and the grey diamonds indicate outlying values (defined as $<Q1 - 1.5 \times IQR$ or $>Q3 + 1.5 \times IQR$). To determine whether there was a significant difference between the AvrM14-A and AvrM14-A^{E82Q} treatments, an unpaired *t*-test was completed and the two-tailed *P*-value is displayed.

Nudix hydrolase structures, we propose that metal ion binding would lock E82 in the solvent-exposed conformation (Gabelli *et al.*, 2002). Overall, the Nudix fold and positioning of the putative metal-binding glutamates suggest that the AvrM14 effectors are enzymatically active Nudix hydrolases.

The RipN and Avr3b effectors both interfere with plant immunity in a Nudix-box-dependent manner, when expressed in *A. thaliana* and *N. benthamiana*, respectively (Dong *et al.*, 2011; Sun *et al.*, 2019). To determine whether AvrM14 can use Nudix hydrolase activity to interfere with plant immunity, we used *Agrobacterium*-mediated transformation in *N. benthamiana* to transiently express AvrM14-A, AvrM14-B, and both proteins with glutamate 82 mutated to glutamine (AvrM14-A^{E82Q} and AvrM14-B^{E82Q}) as YFP fusions and assessed their effect on plant immune responses. Numerous studies have demonstrated this equivalent mutation drastically reduces the catalytic activity of Nudix hydrolases, without altering protein structure or stability (Lin *et al.*, 1996; Perraud *et al.*, 2003; Mildvan *et al.*, 2005; Parrish *et al.*, 2007; Gunawardana *et al.*, 2008; Höfer *et al.*, 2016). Our results demonstrate that the expression of AvrM14-A and AvrM14-B, but not the E82Q mutants, inhibits the production of ROS, following exposure of *N. benthamiana* leaf tissue to either flg-22 or chitin (Fig. 1b). Both AvrM14 and E82Q mutant proteins were expressed and accumulated to similar levels in agroinfiltrated plant tissue (Fig. S2).

As both AvrM14-A and AvrM14-B suppress ROS production, and AvrM14-B is not recognised by the flax M1 and M4 R-proteins, we hypothesised that hydrolase activity would not be required for the recognition of AvrM14-A by M1 and M4. In support of this hypothesis, transient expression of AvrM14-A and AvrM14-A^{E82Q}, but not AvrM14-B or AvrM14-B^{E82Q}, triggered cell-death responses in near-isogenic lines of the flax variety Bison containing either *M1* (*M1* flax) or *M4* (*M4* flax) (Fig. 1c). *M1* and *M4* were introgressed into the Bison genetic background by 12 backcrosses, see Islam & Mayo (1990).

Analogous results were observed in tobacco when the effector was transiently co-expressing with *M1* (Fig. S3). Interestingly, AvrM14-A^{E82Q} expression appeared to result in a stronger cell-death response when compared to the wild-type protein in both *M1* and *M4* flax (Fig. 1c). We confirmed this result by expressing AvrM14-A and AvrM14-A^{E82Q} in a total of 36 *M1* flax leaves per treatment and the HR cell-death response was assessed by determining the mean signal intensity of each infiltrated area following green-light imaging of the leaves (Fig. 1d). The results demonstrate that AvrM14-A^{E82Q} expression results in a greater cell-death response than AvrM14-A (Fig. 1d). Our results indicate that while the integrity of the Nudix box is dispensable for M1 and M4 detection, the AvrM14-A E82Q mutation does influence the severity of the M1 activated immune response. Collectively, these data suggest that AvrM14 can suppress both PTI and ETI pathways, via an unknown Nudix hydrolase activity.

RNA cap analogues and capped RNA transcripts are selectively hydrolysed by AvrM14

To determine the compound(s) hydrolysed by AvrM14, we conducted a comprehensive substrate search, utilising a sensitive

fluorometric assay (Xu *et al.*, 2013), which tested AvrM14-A protein against 69 unique nucleoside diphosphate compounds (listed in Table S3). AvrM14-A only exhibited hydrolysis activity with a single substrate, ^{m7}Gp₅G (P1-(5'-7-methyl-guanosyl)-P5-(5'-guanosyl)-pentaphosphate). AvrM14-A did not hydrolyse diguanosine pentaphosphate (Gp₅G), indicating a preference for the methyl group.

To determine whether substrate hydrolysis was dependent on the Nudix box present in AvrM14-A and conserved in AvrM14-B, we assessed the hydrolytic activity of recombinant AvrM14-A, AvrM14-B, AvrM14-A^{E82Q} and AvrM14-B^{E82Q} against ^{m7}Gp₅G and monitored fluorescence over time (Fig. 2a). AvrM14-A and AvrM14-B hydrolysed ^{m7}Gp₅G, whereas the catalytic site mutants did not (Fig. 2a). ^{m7}Gp₅G is not found in nature; however, 7-methyl guanosine (^{m7}G) is a unique molecular structure present on the 5' cap of eukaryotic RNA transcribed by RNA polymerase II (Müller-McNicoll & Neugebauer, 2014); ^{m7}Gp₅G is used as an mRNA cap analogue in assays. Therefore, the results from the substrate screening experiments suggest that AvrM14 may function as an mRNA-decapping enzyme.

To determine whether the AvrM14 proteins hydrolyse ^{m7}G-capped RNA, we conducted a radiolabelled assay utilising a known decapping enzyme, *Homo sapiens* Nudt16 (HsNudt16) (Song *et al.*, 2010; Li *et al.*, 2011), as a positive control. AvrM14-A and AvrM14-B both efficiently decapped the labelled mRNA substrate, whereas the active site mutants (AvrM14-A^{E82Q} and AvrM14-B^{E82Q}) did not (Fig. 2b). These data demonstrate that AvrM14 is an active Nudix hydrolase with specificity for capped mRNA *in vitro*.

AvrM14 homodimerisation via domain swapping optimises RNA decapping

The AvrM14-A and AvrM14-B crystal structures display a common crystal packing interface despite different crystallisation conditions and crystallographic space groups (Table S2; Fig. S4c). Interestingly, the position of the interface, with respect to the Nudix-box helix, is similar to previously identified homodimeric RNA-decapping enzymes HsNudt16 and X29 (a Nudt16 ortholog from *Xenopus laevis*; Scarsdale *et al.*, 2006; Trésaugues *et al.*, 2015; Fig. S5). We aimed to determine whether homodimerisation of AvrM14 is important for mRNA decapping. Based on SEC (size-exclusion chromatography) chromatograms, we show that both recombinant AvrM14-A and AvrM14-B proteins exist in two stable and distinct oligomeric states that can be purified to near homogeneity (Fig. S4a,b). To determine the molecular mass of each oligomeric state more accurately, we utilised SEC coupled to a multi-angle light-scattering detector (SEC-MALS; Fig. 3). Our SEC-MALS data demonstrate that, in solution, recombinant AvrM14-B forms stable monomers and homodimers, which can be readily separated and purified (Fig. 3a).

The initial crystallisation and activity assays reported above were completed with monomeric AvrM14 proteins, which are the predominant forms after purification from *E. coli* (Fig. S4a). The fact that previous research indicates that HsNudt16 and X29 Nudix hydrolase mRNA-decapping enzymes act as homodimers,

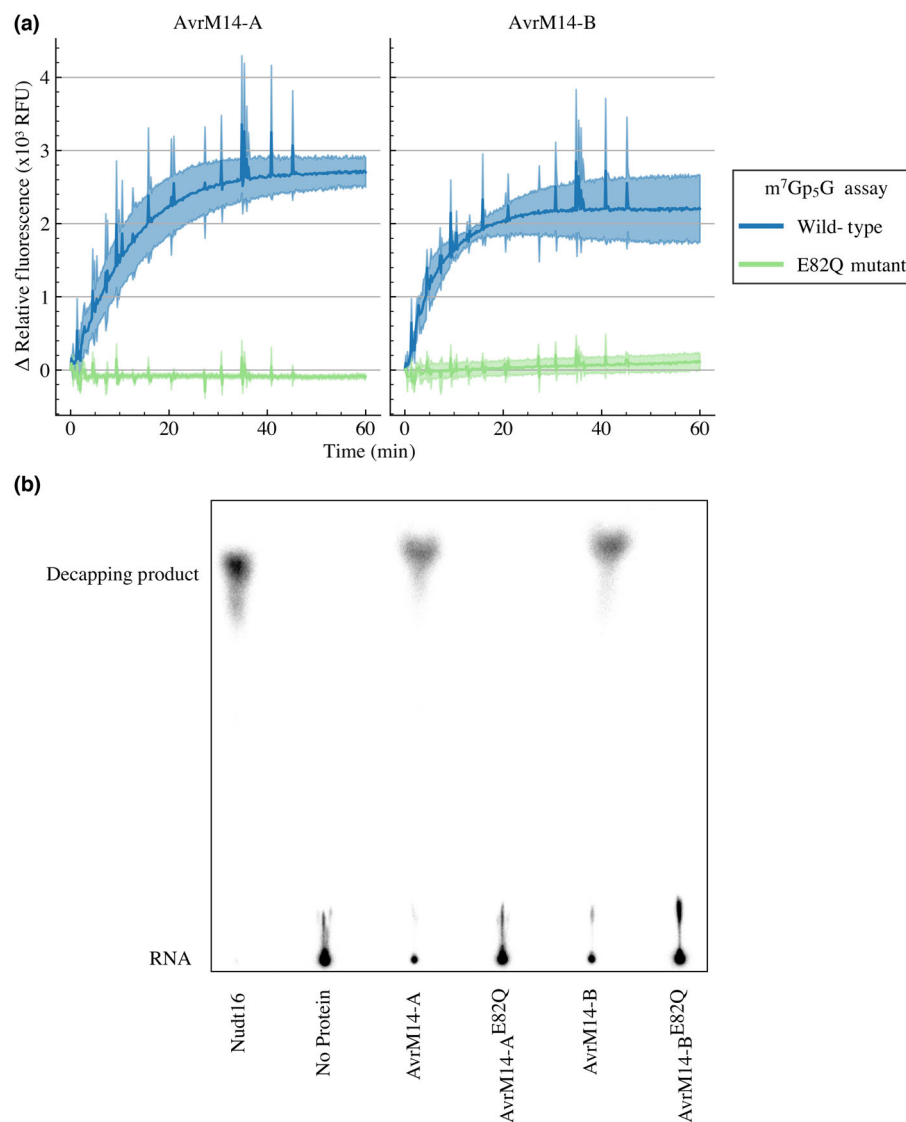


Fig. 2 AvrM14-A and AvrM14-B hydrolyse RNA cap analogues and capped mRNA *in vitro*. (a) Recombinant AvrM14-A (left) and AvrM14-B (right) (data in blue) and the corresponding mutant AvrM14^{E82Q} proteins (green) were incubated with the mRNA cap analogue ^{m7}Gp₅G. Hydrolysis activity was measured over 60 min using a phosphate-binding fluorophore. Results are means (solid line) ± SDs (shaded area), where *n* = 3. (b) Recombinant proteins (HsNudt16, AvrM14-A, AvrM14-A^{E82Q}, AvrM14-B and AvrM14-B^{E82Q}) were incubated with ^{m7}Gp³²pp-RNA and the reaction products analysed by thin-layer chromatography (TLC). Capped RNA remains at the origin of the TLC plate, whereas decapping products (^{m7}GDP and/or ^{m7}GMP) migrate up the plate.

prompted us to further characterise the homodimeric form of AvrM14. To determine whether homodimerisation alters substrate specificity, we performed substrate screening with five common Nudix hydrolase substrates (Fig. S6). Consistent with the monomeric forms of the protein, homodimeric AvrM14-A and AvrM14-B did not hydrolyse any of the substrates tested (Fig. S6). To determine whether homodimeric AvrM14 proteins could decap RNA, we performed activity assays with ^{m7}G-capped RNA. Both AvrM14-A and -B homodimers hydrolysed capped RNA efficiently, whereas homodimeric AvrM14-A^{E82Q} did not (Fig. 3b). Intriguingly, the product produced by the homodimers migrated to a lower position following separation by thin-layer chromatography (TLC), compared with the product released by the monomers (Fig. 3b). To identify the products released by the mRNA-decapping proteins, we measured the migration of ^{m7}GMP, ^{m7}GDP, GMP and GDP standards using UV shadowing under our TLC conditions (Fig. S7). The R_f values recorded for the ^{m7}GMP, ^{m7}GDP, GMP and GDP standards were used to place the labels on Figs 3(b) and 4(d). Our data indicate that the

major product released by homodimeric AvrM14 is ^{m7}GDP, whereas the major product released by monomeric protein is ^{m7}GMP. Thus, mRNA decapping by homodimeric AvrM14 generates 5'-monophosphate RNA (p-RNA), whereas monomeric AvrM14 generates 5'-diphosphate RNA (pp-RNA) (Fig. 3c). To promote mRNA decay, decapping enzymes are hypothesised to release p-RNA *in vivo*, that can be degraded by 5'-3' exoribonucleases, whereas pp-RNA is resistant to exoribonuclease degradation (Fujimura & Esteban, 2010; Schoenberg & Maquat, 2012; Grudzien-Nogalska & Kiledjian, 2017). Our *in vitro* results therefore suggest that to promote host mRNA decay, AvrM14 would function as a homodimer.

To understand how the AvrM14 proteins homodimerise, we sought to determine the crystal structure of homodimeric AvrM14-B. To ensure any differences observed in the structure were independent of the crystallisation process, we crystallised homodimeric AvrM14-B in identical conditions to monomeric AvrM14-B. The crystal structure demonstrates that homodimerisation is mediated by domain swapping (Fig. 3d). The

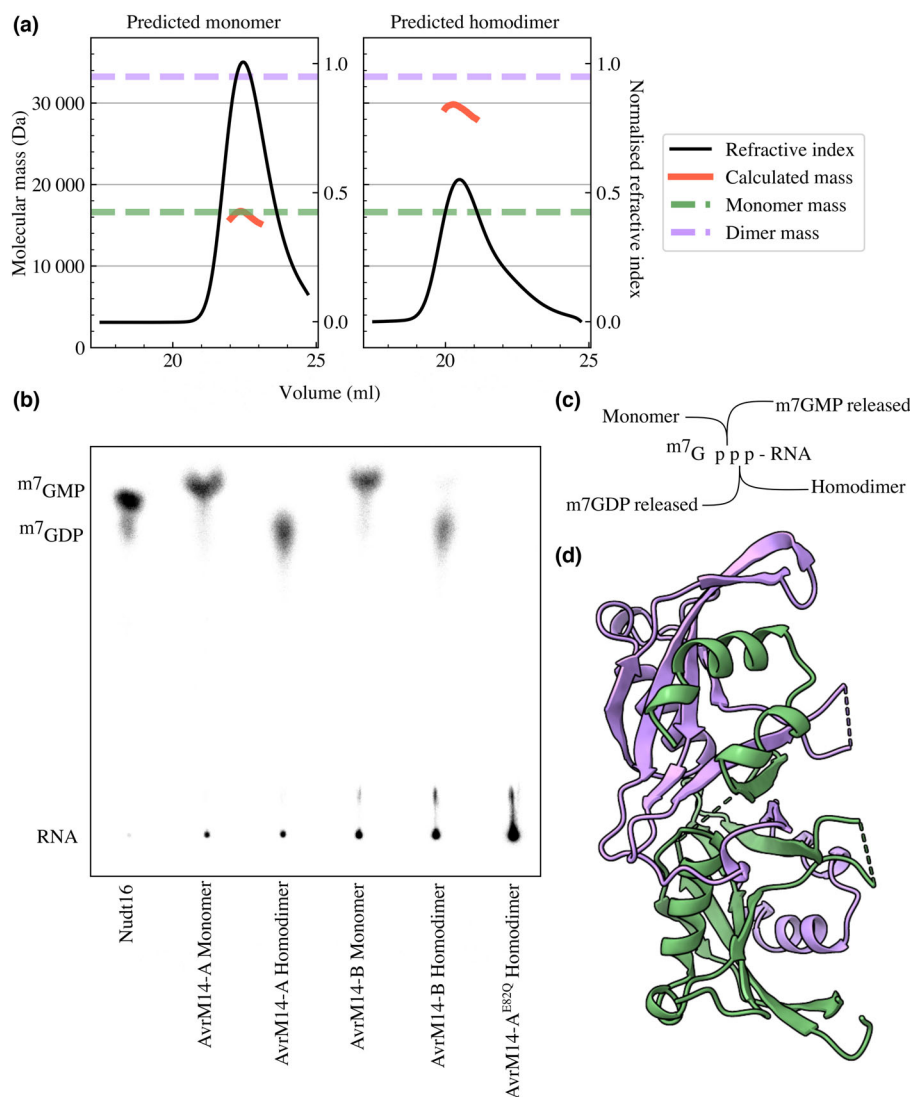


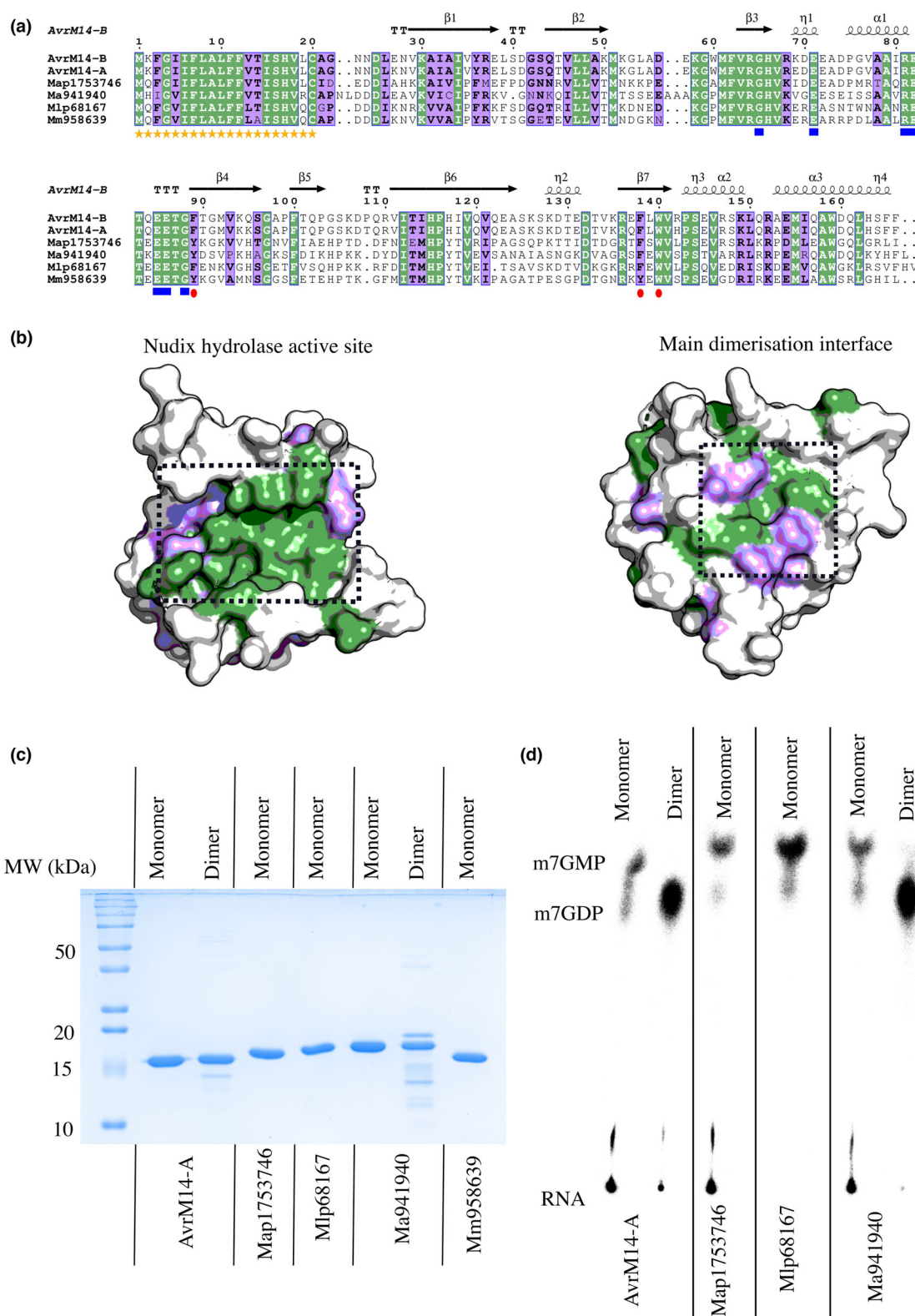
Fig. 3 Homodimerisation of AvrM14 is mediated by domain swapping, which alters RNA cap-cleavage location, compared with the monomer. (a) Size-exclusion chromatography coupled with multi-angle light scattering (SEC-MALS) was used to determine the molecular mass of the different oligomeric forms of AvrM14-B in solution. For all plots, the black lines refer to the right y-axis and indicate the protein elution traces (normalised refractive index) for proteins eluted from the Superdex S75 10/300 increase column. The red bands correspond to the average molecular-mass distribution across the refractive index peak, all molecular masses refer to the left y-axis. The green and purple dashed lines indicate the theoretical molecular mass of monomeric (16.6 kDa) and homodimeric (33.2 kDa) AvrM14 protein, respectively. (b) The separate monomeric and homodimeric forms of AvrM14-A and AvrM14-B were incubated with $m^7Gp^{32}pp$ -RNA and the reaction products were separated using thin-layer chromatography. HsNudt16 was included as a positive control. The predicted identity of each ^{32}P -labelled compound is indicated on the left, based on the Rf value determined for standard solutions of m^7GMP and m^7GDP . (c) The pyrophosphate bond predominantly hydrolysed by monomeric and homodimeric AvrM14 proteins based on the RNA cap-cleavage assay results. (d) Ribbon model of the crystal structure of homodimeric AvrM14-B (PDB ID: 8DPA), showing C-terminal domain swapping. Chain A is coloured green and chain B purple.

C-terminal regions (residues 124 to 166) from each of the monomeric proteins swap positions to form an intertwined homodimer (Fig. 3d). Domain-swapped homodimeric structures have been reported previously for ADPR-specific Nudix hydrolases (Gabelli *et al.*, 2001; Kang *et al.*, 2003; Yoshida *et al.*, 2004; Zha *et al.*, 2006; Wakamatsu *et al.*, 2008; Tang *et al.*, 2015). However, the position of each monomeric subunit in the AvrM14 structure differs substantially from the previously reported domain-swapped Nudix hydrolases. The overall positioning of each monomeric subunit and the corresponding dimerisation interface are almost identical to the crystal packing observed in the asymmetric units of monomeric AvrM14-A and AvrM14-B and therefore are similar to the HsNudt16/X29 homodimers (Figs 3d, S4c, S5). Buried in the main interface between the two monomeric subunits is an aromatic core composed of F⁸⁹, F¹³⁸ and W¹⁴⁰ from both monomers, which we hypothesise promote self-association (Fig. S4c). We attempted to mutate these amino acids to prevent homodimerisation for further experiments; however, the mutant proteins were not stable when expressed in *E. coli*.

To investigate whether stable dimeric forms of AvrM14 are produced *in planta*, we performed native protein extractions from *N. benthamiana* tissue expressing untagged AvrM14 protein. We separated these proteins using SEC, followed by western blot analysis with specific polyclonal antibodies raised against AvrM14 protein (Fig. S8). Using this approach, we observed AvrM14 protein elution from SEC at a volume consistent with monomeric forms of the protein. These data suggest that AvrM14 does not form stable dimers *in planta*, mediated by the domain-swapping mechanism observed in *E. coli*. However, these results do not preclude the potential for AvrM14 to function as a homodimer via transient association with other proteins that cannot be detected using these methods.

RNA-decapping activity is conserved in Nudix effectors from other pathogenic *Melampsora* spp.

We next wanted to determine whether other plant pathogens secrete similar Nudix hydrolase effectors with RNA-decapping activity. BLAST searches with JGI and NCBI databases yielded



proteins homologous to *AvrM14* from all genome-sequenced *Melampsora* species. Their sequence identity to the *AvrM14* proteins is *c.* 50%, with all sequences demonstrating conservation of the signal peptide, Nudix box and residues involved in the

dimerisation interface (Fig. 4a). Mapping the sequence conservation onto the structure of monomeric *AvrM14-B* demonstrates extremely high conservation around the Nudix hydrolase active site, suggesting that the homologues are active Nudix hydrolases

Fig. 4 Predicted effectors homologous to AvrM14 from multiple *Melampsora* species decap RNA *in vitro*. (a) Sequence alignment (produced using ESPRIT 3.0) of AvrM14 variants and homologous proteins from other *Melampsora* species (Robert & Gouet, 2014). Each sequence is labelled with the relevant unique protein ID from the JGI database and the first letter of their genus and species name (Mm for *Melampsora medusae*, Mlp for *Melampsora larici-populina*, Map for *Melampsora allii-populina*, and Ma for *Melampsora americana*). Residues with 100% conservation are coloured green, residues with conserved substitutions are coloured purple, white are nonconserved residues, the predicted signal peptide region is indicated by orange stars, the aromatic residues in the AvrM14 dimeric interface are indicated by red dots, and the conserved Nudix box residues are indicated by blue squares. Above the sequence alignment is the secondary structure of AvrM14-B (black arrows indicating β -strands, squiggles indicating helices, and the TT and TTT symbols indicating β -turns and α -turns respectively). (b) The structure of monomeric AvrM14-B, demonstrating the surface regions with the highest conservation across the homologues. Residue colouring is the same as in the sequence alignment. The Nudix hydrolase active site and the major interface involved in dimerisation are indicated. (c) Coomassie-stained SDS-PAGE analysis demonstrating the purity of each protein used in the RNA-decapping assays. (d) Recombinant AvrM14-A and the homologous proteins were incubated with ^{32}P -Gp-pp-RNA and the reaction products were separated using thin-layer chromatography. The oligomeric state of each protein, as predicted by size-exclusion chromatography, is indicated along the top. The predicted identity of each ^{32}P labelled compound is indicated on the left, based on the Rf value determined for standard solutions of ^{32}P -GMP and ^{32}P -GDP. A middle lane not relevant to the analysis has been removed from the image.

featuring similar substrate specificity (Fig. 4b). The surface involved in dimerisation is also highly conserved (Fig. 4b). No Nudix hydrolases with similarity to AvrM14 were identified outside of the genus *Melampsora*.

The predicted AvrM14 homologues from *Melampsora americana*, *Melampsora medusae*, *Melampsora allii-populina* and *Melampsora larici-populina* were selected for biochemical analysis (sequences in Table S1). Size-exclusion chromatography indicated that all homologues were predominantly in a monomeric state, following purification from *E. coli* (Fig. S9). All monomeric proteins could be purified to near homogeneity and decapped mRNA *in vitro* (Fig. 5). The assay results demonstrate that RNA-decapping activity has been conserved throughout the evolution of this gene family in *Melampsora* spp. The AvrM14 homologues from all species, except *M. medusae*, also showed a SEC absorbance peak at a position consistent with a homodimeric protein (Fig. S9). However, low yields of the putative homodimeric proteins meant that only one (the homologue from *M. americana*) could be purified (Fig. 4c). Analogous to homodimeric AvrM14 from *M. lini*, the homologous *M. americana* homodimer released predominantly ^{32}P -GDP from capped RNA *in vitro*, whereas the monomeric protein released predominantly ^{32}P -GMP (Fig. 4d).

AvrM14 expression in flax promotes the expression of genes involved in growth and metabolic processes while inhibiting aspects of plant immunity

To better characterise how the AvrM14 effector impacts host plant physiology, we transiently expressed AvrM14-A in flax leaves and conducted transcriptome-wide RNA-sequencing (RNA-Seq) analysis. The RNA was extracted from leaves recently infiltrated with *Agrobacterium*, to enable AvrM14 expression. Therefore, our data are representative of the changes induced by AvrM14 following the activation of plant immune responses by *Agrobacterium* exposure. Our differential expression (DE) analysis identified 488 and 312 significantly (q value < 0.05) more abundant ($\log_2\text{fc} > 0.5$) and less abundant ($\log_2\text{fc} < -0.5$) transcripts, respectively, in leaves agroinfiltrated with AvrM14-A, compared with the vector-only control (Table S4). Gene Ontology (GO) enrichment analysis indicates that AvrM14 expression promotes the expression of genes involved in carbon fixation, photosynthetic reactions and various metabolic processes (Fig. 5a), and suppresses the expression of genes involved in cell-

cell recognition, hypoxia, salt and biotic stress responses (Fig. 5a). To identify which changes are due to the enzymatic activity of AvrM14, we also conducted RNA-Seq on flax leaves expressing AvrM14-A^{E82Q} and compared the AvrM14-A and AvrM14-A^{E82Q} datasets. Both AvrM14-A and AvrM14-A^{E82Q} were expressed at similar levels (Fig. S10). The DE analysis indicates that many of the differences between the AvrM14-A and vector-only datasets are unrelated to enzymatic activity, with only 90 significantly more abundant and 36 significantly less abundant transcripts in leaves agroinfiltrated with AvrM14-A, compared with AvrM14-A^{E82Q} (Table S5). There is multiple significantly less abundant transcripts homologous to pseudo-response regulator 5 (APRR5) from *A. thaliana* (Fig. 5b). Consistent with changes to APRR5 levels, there is an overrepresentation of transcripts homologous to *A. thaliana* APRR5 targets (Nakamichi *et al.*, 2012) in the significantly less abundant transcripts (Fig. 5c). APRR5 is an important regulator of *A. thaliana* circadian rhythm (Nakamichi *et al.*, 2005; Rawat *et al.*, 2011); our results therefore suggest that the enzymatic activity of AvrM14 effectors could impact circadian rhythm processes.

Surface-exposed residues required for M1 and M4 recognition

In addition to characterising the virulence function of AvrM14, we were interested in understanding the requirements for recognition of AvrM14 by M1 and M4. Flax M1 belongs to the TIR-NLR class of R-proteins. M4 has not yet been cloned, but is expected to encode a protein closely related to M1 (Lawrence *et al.*, 2010).

The AvrM14 structures reveal that the six amino acid polymorphisms differentiating the A and B alleles map to the protein surface (Fig. 6a). To understand which polymorphisms are important for recognition, we transiently expressed various AvrM14 proteins with single or double mutations at the six polymorphic residues in tobacco co-expressing M1 (M1 tobacco) and in near-isogenic lines of the flax variety Bison containing either M1 (M1 flax) or M4 (M4 flax), using *Agrobacterium*-mediated transformation (sequences in Table S1).

The expression and accumulation of all mutant AvrM14 proteins in plant tissue were confirmed via Western blotting (Fig. S2). Most of the mutations had only a minor or no effect on the observed phenotype (Figs S11, S12; Table S6). Only by

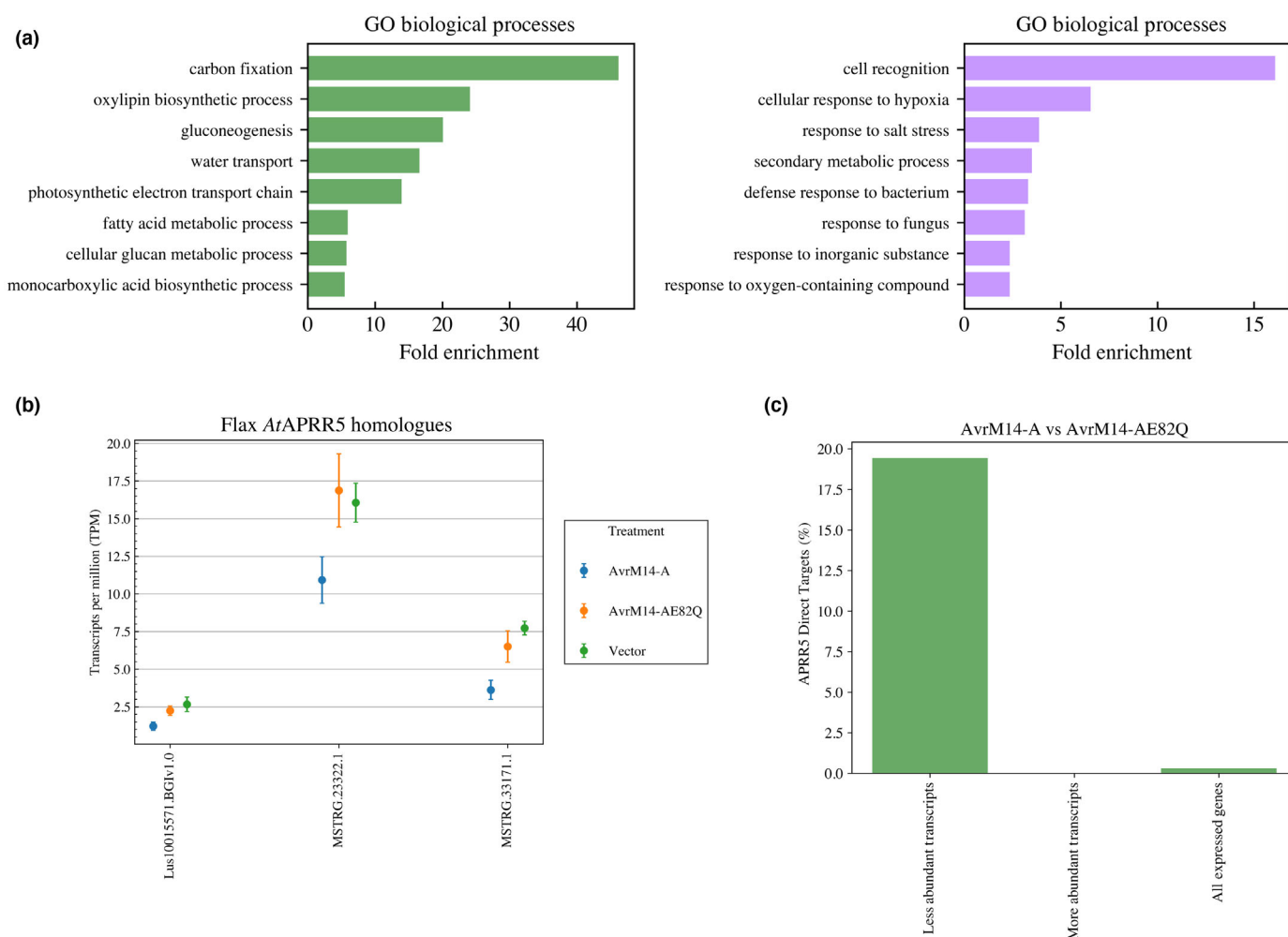


Fig. 5 Enzymatic activity of AvrM14-A in flax leaves reduces the relative abundance of transcripts homologous to *Arabidopsis thaliana* APRR5 and APRR5 direct targets. (a) The Gene Ontology biological processes that are enriched (FDR < 0.05) in the list of transcripts significantly ($q < 0.05$) more abundant (left, green; $\log_2\text{fc} > 0.5$) and less abundant (right, purple; $\log_2\text{fc} < -0.5$), when comparing flax leaves transformed with AvrM14-A to an empty vector. Only the top 10 (sorted by fold enrichment) processes are shown, after filtering out redundant terms using REVIGO (Supek *et al.*, 2011). (b) The average expression levels (\pm SDs) are displayed as transcripts per million (TPM) for transcripts homologous to *A. thaliana* PRR5 that are significantly less abundant ($q < 0.05$, $\log_2\text{fc} < -0.5$) when comparing the AvrM14-A (blue) ($n = 4$) and AvrM14-A^{E82Q} (orange) ($n = 4$) RNA-Seq datasets, the mean TPM (\pm SDs) are also displayed for the vector-only dataset (green) ($n = 3$). The x-axis label indicates the name of the transcript as listed in Tables S4 and S5. (c) The percentage of transcripts homologous to *A. thaliana* APRR5 direct targets, as identified by Nakamichi *et al.* (2012), present in the list of transcripts significantly ($q < 0.05$) less abundant (left; $\log_2\text{fc} < -0.5$), or more abundant (middle) ($\log_2\text{fc} > 0.5$) when comparing flax leaves expressing AvrM14-A to leaves expressing AvrM14-A^{E82Q}. The percentage of transcripts homologous to *A. thaliana* APRR5 direct targets present among all expressed genes included in the differential expression analysis is indicated on the right.

mutating residues 95 and 108, we were able to completely and consistently reverse recognition by both *M1* and *M4* in flax (i.e. AvrM14-A^{K95Q/T108P} expression resulted in a HR similar to AvrM14-B expression and AvrM14-B^{Q95K/P108T} expression resulted in a HR similar to AvrM14-A expression; Fig. 6c; Table S6).

Overall, our results indicate that both *M1* and *M4* R-proteins recognise AvrM14-A using a mechanism that can be evaded by mutating residues 95 and 108, suggesting that the currently uncharacterised *M4* is highly similar to *M1*, consistent with the observation that *M1* and *M4* are likely to be allelic (Lawrence *et al.*, 2010). According to the crystal structure of monomeric and homodimeric AvrM14, residues 95 and 108 do not localise to the same surface region (Fig. 6b). If *M1* and *M4* interact

directly with AvrM14, our results suggest that the R-proteins have multiple contact points with the effector, like previous data suggest occurs with other flax/flax rust R-protein/effector pairs, AvrM and M, and AvrL567 and L5/L6 (Ravensdale *et al.*, 2012; Ve *et al.*, 2013).

Discussion

In this study, we have demonstrated that the AvrM14 effector from *M. lini* is a Nudix hydrolase that is able to suppress plant immunity, modify host transcriptome composition and uncap mRNAs in a manner that would render them susceptible to degradation by host exoribonucleases. No plant pathogens have been previously reported to use mRNA-decapping enzymes to

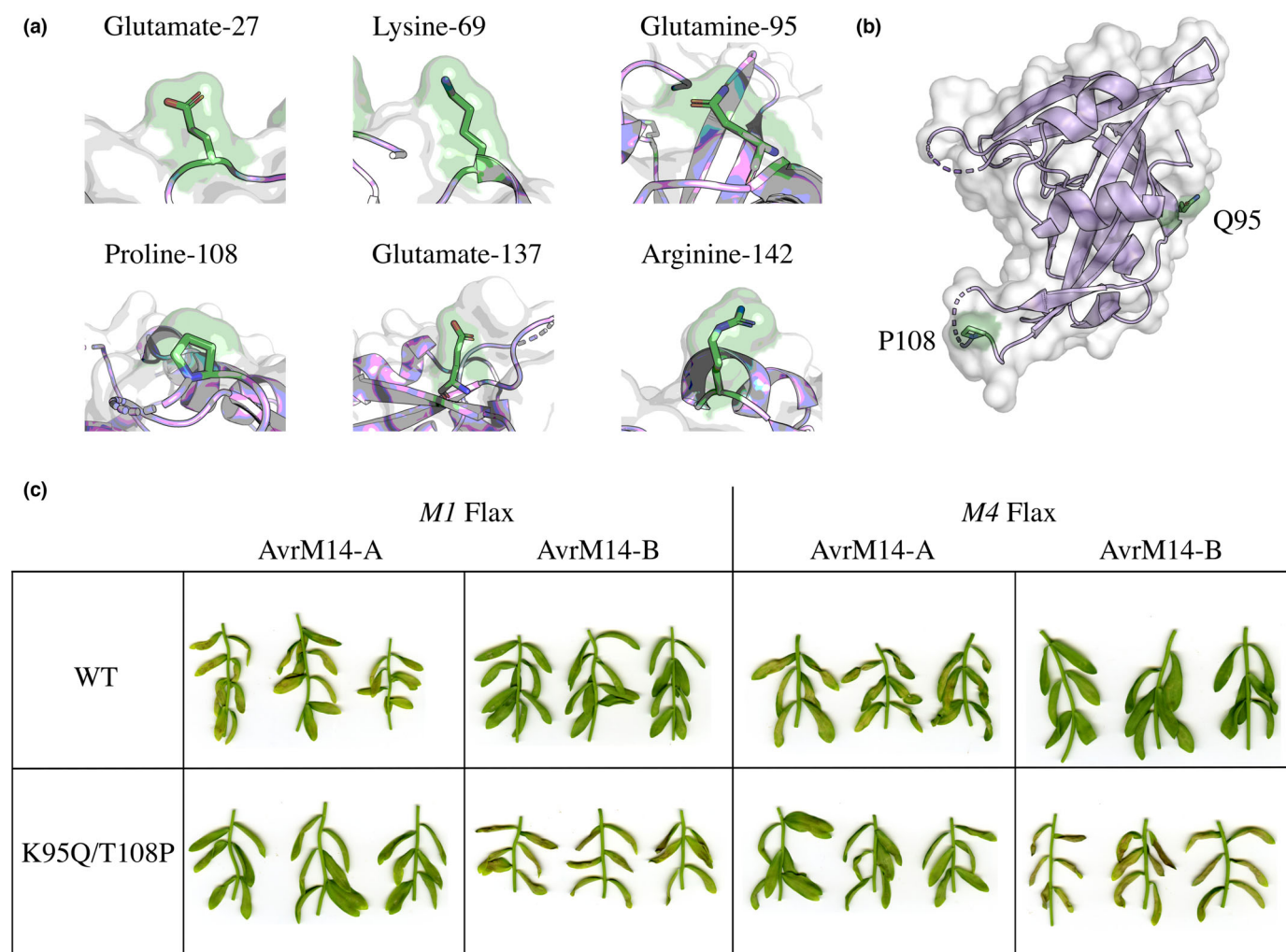


Fig. 6 AvrM14 polymorphic residues are surface-exposed, with residues 95 and 108 involved in resistance protein recognition. (a) The six polymorphic residues differentiating AvrM14-A and AvrM14-B all localise to the protein surface, as demonstrated here using the AvrM14-B structure displayed in ribbon representation, superimposed on a surface representation, with side chains of polymorphic residues coloured green. (b) The crystal structure of AvrM14-B with the side chains of residues important for evading M1 and M4 detection (Q95 and P108) coloured green. (c) Bison \times M1 (Williston Brown) or M4 (Victory 'A') flax (*Linum usitatissimum*) lines were infiltrated with *Agrobacterium* harbouring constructs encoding either wild-type or mutant YFP-tagged AvrM14 proteins (AvrM14-A, AvrM14-B, AvrM14-A^{K95Q/T108P} or AvrM14-B^{Q95K/P108T}). The agroinfiltrated leaves were photographed 5 d postinfiltration to assess the cell-death response.

inhibit plant immunity. Before the present study, only certain animal viruses, including vaccinia and African swine fever viruses, have been known to produce mRNA-decapping Nudix hydrolases during host-cell infection (Parrish & Moss, 2006; Quintas *et al.*, 2017). Our findings have implications for understanding genetic post-transcriptional regulation in plants, in addition to helping understand how *Melampsora* pathogens circumvent plant immunity during successful infection.

Host and pathogen Nudix hydrolases influence plant immunity

Diverse pathogens of plants secrete effectors with Nudix domains and prior research have confirmed that two of these (Avr3b and RipN) can inhibit plant immune function (Dong *et al.*, 2011; Dong & Wang, 2016; Sun *et al.*, 2019). We have demonstrated

that a third effector, AvrM14 from flax rust, is also a Nudix hydrolase that can suppress plant immunity. The Nudix hydrolase activity of AvrM14 inhibits the MAMP-induced ROS burst in the nonhost plant *N. benthamiana* and reduces the HR cell-death response triggered by M1 in flax. However, it is currently unknown whether the suppressive effect of AvrM14 on plant immunity promotes the virulence of flax rust during infection.

Plant Nudix hydrolases also play important roles in regulating plant immune responses. *Arabidopsis thaliana* Nudix hydrolases 6, 7 and 8 (AtNUDX6/7/8) have all been implicated in modulating plant immune function (Bartsch *et al.*, 2006; Ge *et al.*, 2007; Ishikawa *et al.*, 2010; Fonseca & Dong, 2014). Additionally, wheat Nudix hydrolase 23 (TaNUDX23) suppresses ROS accumulation and is stabilised by an effector protein from *Puccinia striiformis* f. sp. *tritici* (Yang *et al.*, 2020). Recently, it was reported that AtNUDX7 and the Avr3b effector can degrade

cyclic nucleotide monophosphates (cNMPs) by acting as phosphodiesterases (Yu *et al.*, 2022). Yu *et al.* (2022) demonstrated that cNMPs are important for TIR-NLR-mediated plant immunity and that NUDX7 can suppress the cell-death response triggered by the TIR-only disease R-protein RBA1 (Yu *et al.*, 2022). AvrM14 does not hydrolyse similar substrates to AtNUDX7, TaNUDX23 or Avr3b *in vitro* and is not structurally similar to AtNUDX7 (Tang *et al.*, 2015); our data support a different mechanism of immunity suppression.

AvrM14 is a highly selective Nudix hydrolase

Nudix hydrolases are renowned for their broad substrate specificity, with many enzymes readily hydrolysing multiple substrates *in vitro* (McLennan, 2013). Avr3b, AtNUDX7, TaNUDX23 and RipN were tested against a limited subset of potential substrates and all hydrolysed multiple substrates (Ogawa *et al.*, 2005; Dong *et al.*, 2011; Sun *et al.*, 2019; Yang *et al.*, 2020), complicating the identification of physiologically relevant substrates. By contrast, we found that AvrM14 does not exhibit broad substrate specificity *in vitro*, based on extensive screening of a total of 70 potential substrates. AvrM14 only hydrolysed mRNA cap analogues and capped mRNA. In our broad screen, AvrM14 effectively hydrolysed ^{m7}Gp₅G but not Gp₅G, suggesting that AvrM14 achieves substrate specificity by selecting for the methylated guanosine. Nudix hydrolases with specificity for methylated guanosine have been reported previously and experimental evidence indicates that these proteins function as mRNA-decapping enzymes (Van Dijk *et al.*, 2002; Wang *et al.*, 2002; Piccirillo *et al.*, 2003; Parrish *et al.*, 2007; Parrish & Moss, 2007). The canonical mRNA-decapping enzyme in eukaryotes, DCP2, demonstrates improved mRNA-decapping activity with ^{m7}Gp₃RNA, when compared to Gp₃RNA (Van Dijk *et al.*, 2002; Wang *et al.*, 2002; Piccirillo *et al.*, 2003). Additionally, two mRNA-decapping enzymes from the vaccinia virus, D9 and D10, both demonstrate specificity for methylated guanosine substrates (Parrish *et al.*, 2007; Parrish & Moss, 2007). Structural studies with mRNA cap analogues indicate that the N-terminal regulatory domain (NRD) of DCP2 is important for binding to the cap region (Charenton *et al.*, 2016; Mugridge *et al.*, 2016; Wurm *et al.*, 2017). AvrM14 lacks an NRD, therefore binding cannot be controlled by the same mechanism as DCP2. We attempted cocrystallisation of AvrM14 with the mRNA cap analogues ^{m7}Gp₃G and ^{m7}Gp₅G to understand the molecular basis of substrate selectivity, but were unable to capture them bound to the enzyme.

AvrM14 likely functions as a homodimer to ensure the correct mRNA cap pyrophosphate bond is hydrolysed

We found that a proportion of AvrM14 protein was produced in *E. coli* as a stable dimer and demonstrated via X-ray crystallography that this was mediated via domain swapping. Dimerisation via domain swapping has been shown previously for other Nudix hydrolases (Gabelli *et al.*, 2001; Kang *et al.*, 2003; Yoshida *et al.*, 2004; Zha *et al.*, 2006; Wakamatsu *et al.*, 2008; Tang

et al., 2015), and we were interested in investigating the biological relevance of this, if any, for AvrM14. Our *in planta* experiments show that AvrM14 is monomeric when expressed in *N. benthamiana*, indicating that homodimerisation of AvrM14 via the domain-swapping mechanism in plants is unlikely. Unfortunately, the method we used to discriminate monomeric and homodimeric AvrM14 is not sensitive enough to investigate what the fungus itself delivers into flax cells during infection. Despite this, we suggest that AvrM14 functions as a dimer to decap mRNA. Our *in vitro* and *in silico* analyses provide multiple lines of evidence for AvrM14 functioning as a homodimer. We demonstrate that homodimeric AvrM14 releases ^{m7}GDP and 5'-monophosphate RNA from capped mRNA. It is well established that following decapping, mRNA transcripts in cells are subject to 5'-3' decay by exoribonucleases (XRN4 in plants), which target a 5' end monophosphate RNA substrate, and that 5' diphosphate RNA is not a direct target for 5' decay (Grudzien-Nogalska & Kiledjian, 2017). In support of this, the structurally related decapping enzyme Nudt16, homodimerises and preferentially releases ^{m7}GDP (Song *et al.*, 2010, 2013; Trésaugues *et al.*, 2015). There are also strong similarities between the homodimerisation interface observed in the Nudt16 crystal structure (PDB ID: 3MGM) and the crystal packing, and domain-swap dimer, observed for AvrM14-A and AvrM14-B. In addition, the aromatic residues involved in the dimeric interface of AvrM14 are highly conserved in homologous effectors from other *Melampsora* species, suggesting that this protein-protein interaction surface is important for effector function. Collectively, based on our *in vitro* and *in silico* analysis of AvrM14 and the homologous effectors, we suggest that these proteins are biologically active as dimers, but how this is achieved in a natural setting, that is domain swapping, interactions with other proteins or mRNA itself, remain unknown.

Controlling plant immunity by decapping mRNA

AvrM14 decaps mRNA *in vitro* and the mRNA-decapping activity requires glutamate-82 (E82). We also demonstrated that E82 is required for suppression of ROS production in *N. benthamiana* and for the reduction in the cell-death response following AvrM14 recognition by M1 in flax. Our results are consistent with AvrM14 acting as an mRNA-decapping enzyme, to inhibit aspects of plant immunity. This suggests that AvrM14 can selectively decap transcripts involved in plant immunity, rather than destabilising the entire transcriptome. We speculate that AvrM14 may interact with other proteins in the plant cell to enable transcript selectivity, as occurs with DCP2 in yeast (He *et al.*, 2018). Alternatively, AvrM14 may be hydrolysing another unknown compound *in planta* that also requires E82 to inhibit plant immunity. However, due to the selectivity of AvrM14 for methylated guanosine substrates *in vitro*, our substrate screening data suggest that this is unlikely.

The decapping and decay of plant mRNA are known to be important for plant immune function. For example, following immune activation, phosphorylation of the DCP2-interacting protein DCP1 (decapping 1) enhances DCP2-dependent decay

of multiple transcripts encoding negative regulators of plant immunity (Yu *et al.*, 2019; He *et al.*, 2022). By contrast, during periods of normal growth, mRNA decapping and decay can prevent immune activation via nonsense-mediated mRNA decay (NMD) of numerous *R*-gene transcripts (Gloggnitzer *et al.*, 2014; Jung *et al.*, 2020). Nonsense-mediated mRNA decay regulation for many of these *R*-genes requires VARICOSE (VCS), a scaffolding protein for decapping machinery (Xu *et al.*, 2006; Raxwal *et al.*, 2020).

Our RNA-Seq analysis identified that the enzymatic activity of AvrM14-A decreases the abundance of multiple transcripts homologous to *A. thaliana* circadian network-related genes. Plant defence responses, including ROS production and the HR triggered by R-proteins, are linked to circadian rhythm (Lu *et al.*, 2017; Westwood *et al.*, 2019; Butt *et al.*, 2020). For example, the expression of some *A. thaliana* *R*-genes is controlled by the circadian regulator, CIRCADIAN CLOCK-ASSOCIATED 1 (Wang *et al.*, 2011) and the amplitude of ROS production following flg-22 exposure is time-of-day-dependant (Korneli *et al.*, 2014). The suppression of ROS production and reduction in the M1-activated HR by the enzymatic activity of AvrM14 may be a result of AvrM14 altering plant circadian rhythm.

The transcript level of regulators of circadian rhythm in *A. thaliana* has recently been identified to be controlled by 5′–3′ mRNA decay requiring the cytoplasmic exoribonuclease XRN4 (Carenio *et al.*, 2022). We speculate that AvrM14 decreases the abundance of flax circadian rhythm regulator transcripts by removing their 5′ cap and promoting their XRN4-dependant decay. Further research is required to confirm that the decrease in the abundance of APRR5 and other circadian-rhythm-related transcripts due to the enzymatic activity of AvrM14 is a direct result of these transcripts being decapped by AvrM14.

Acknowledgements

This work was supported by funding from the Australian Research Council (ARC) (Discovery Projects DP120100685, DP160102244 and DP200100387) and the Australian National University (ANU) Future Scheme (35665). SW was supported by ARC DECRA (DE160100893) and Future Fellowships (FT200100135). BK was supported by a Laureate Fellowship (FL180100109). CM and DY were recipients of the Australian Government Research Training Programme (RTP) Stipend Scholarship and the Australian Institute of Nuclear Science and Engineering (AINSE) Ltd. Postgraduate Research Award (PGRA). We thank Ayesha Akram for providing mature flax plants for the RNA-Seq experiment, and the Plant Services Team at the Australian National University for providing *Nicotiana benthamiana* seedlings. We thank Jeffrey Ellis for support during the early stages of the work and scientific discussion. The authors acknowledge the use of the ANU crystallisation facility. The authors also acknowledge the use of the Australian Synchrotron MX facility and thank the staff for their support. This research was undertaken in part using the MX2 beamline at the Australian Synchrotron, part of ANSTO, and made use of the Australian Cancer Research Foundation (ACRF) detector. Open access

publishing facilitated by Australian National University, as part of the Wiley - Australian National University agreement via the Council of Australian University Librarians.

Competing interests

None declared.

Author contributions

CLM, A-MC, PND, BK, DAJ and SJW planned and designed the research study. CLM, A-MC, JRG, AMD, MAO, DSY and SJW performed the experiments; CLM, A-MC, JRG, DJE, SEB, PND, DAJ and SJW analysed the data. CLM wrote the original draft and all authors contributed to writing, reviewing and editing of the manuscript. CLM and A-MC contributed equally to this work.

ORCID

Steven E. Brenner  <https://orcid.org/0000-0001-7559-6185>
Ann-Maree Catanzariti  <https://orcid.org/0000-0001-8518-044X>
Peter N. Dodds  <https://orcid.org/0000-0003-0620-5923>
Daniel J. Ericsson  <https://orcid.org/0000-0001-5101-9244>
Julian R. Greenwood  <https://orcid.org/0000-0003-0497-0541>
David A. Jones  <https://orcid.org/0000-0001-8809-5822>
Bostjan Kobe  <https://orcid.org/0000-0001-9413-9166>
Carl L. McCombe  <https://orcid.org/0000-0001-9347-8879>
Megan A. Outram  <https://orcid.org/0000-0003-4510-3575>
Simon J. Williams  <https://orcid.org/0000-0003-4781-6261>
Daniel S. Yu  <https://orcid.org/0000-0003-0454-7989>

Data availability

The data that support the protein structures described in this study are openly available under accession nos. 8DP8, 8DP9 and 8DPA at the PDB. RNA-sequencing data are available from the NCBI (GEO: GSE207874, SRA: SRX16112399, SRX16112400, SRX16112401, SRX16112402, SRX16112403, SRX16112404, SRX16112405, SRX16112406, SRX16112384, SRX16112385 and SRX1611238).

References

- Afonine PV, Grosse-Kunstleve RW, Echols N, Headd JJ, Moriarty NW, Mustyakimov M, Terwilliger TC, Urzhumtsev A, Zwart PH, Adams PD. 2012. Towards automated crystallographic structure refinement with phenix.refine. *Acta Crystallographica. Section D, Biological Crystallography* **68**: 352–367.
- Ames BN. 1966. Assay of inorganic phosphate, total phosphate and phosphatases. In: *Methods in enzymology*. Cambridge, MA, USA: Academic Press, 115–118.
- Anderson C, Khan MA, Catanzariti A-M, Jack CA, Nemri A, Lawrence GJ, Upadhyaya NM, Hardham AR, Ellis JG, Dodds PN *et al.* 2016. Genome analysis and avirulence gene cloning using a high-density RADseq linkage map of the flax rust fungus, *Melampsora lini*. *BMC Genomics* **17**: 667–668.

- Aragão D, Aishima J, Cherukuvada H, Clarksen R, Clift M, Cowieson NP, Ericsson DJ, Gee CL, Macedo S, Mudie N. 2018. MX2: a high-flux undulator microfocus beamline serving both the chemical and macromolecular crystallography communities at the Australian Synchrotron. *Journal of Synchrotron Radiation* 25: 885–891.
- Bartsch M, Gobatto E, Bednarek P, Debey S, Schultze JL, Bautor J, Parker JE. 2006. Salicylic acid-independent ENHANCED DISEASE SUSCEPTIBILITY1 signaling in *Arabidopsis* immunity and cell death is regulated by the monooxygenase *FMO1* and the Nudix hydrolase *NUDT7*. *Plant Cell* 18: 1038–1051.
- Benthall AR, Youles M, Mendel MN, Varden FA, JCDI C, Banfield MJ. 2021. pOPIN-GG: a resource for modular assembly in protein expression vectors. *BioRxiv*. doi: [10.1101/2021.08.10.455798](https://doi.org/10.1101/2021.08.10.455798).
- Bessman MJ, Walsh JD, Dunn CA, Swaminathan J, Weldon JE, Shen J. 2001. The gene *ygdP*, associated with the invasiveness of *Escherichia coli* K1, designates a Nudix hydrolase, Orf176, active on adenosine-pentaphospho-(5')-adenosine (Ap5A). *The Journal of Biological Chemistry* 276: 37834–37838.
- Bhadauria V, Banniza S, Vandenberg A, Selvaraj G, Wei Y. 2013. Overexpression of a novel biotrophy-specific *Colletotrichum truncatum* effector, CtNUDIX, in hemibiotrophic fungal phytopathogens causes incompatibility with their host plants. *Eukaryotic Cell* 12: 2–11.
- Butt GR, Qayyum ZA, Jones MA. 2020. Plant defence mechanisms are modulated by the circadian system. *Biology* 9: 454.
- Careno DA, Santangelo SP, Macknight RC, Yanovsky MJ. 2022. The 5'–3' mRNA decay pathway modulates the plant circadian network in *Arabidopsis*. *Plant & Cell Physiology* 63: 1709–1719.
- Casañal A, Lohkamp B, Emsley P. 2020. Current developments in Coot for macromolecular model building of electron cryo-microscopy and crystallographic data. *Protein Science* 29: 1069–1078.
- Casey LW, Lavrencic P, Benthall AR, Cesari S, Ericsson DJ, Croll T, Turk D, Anderson PA, Mark AE, Dodds PN *et al.* 2016. The CC domain structure from the wheat stem rust resistance protein Sr33 challenges paradigms for dimerization in plant NLR proteins. *Proceedings of the National Academy of Sciences, USA* 113: 12856–12861.
- Catanzari A-M, Lim GTT, Jones DA. 2015. The tomato I-3 gene: a novel gene for resistance to Fusarium wilt disease. *New Phytologist* 207: 106–118.
- Charenton C, Taverniti V, Gaudon-Plesse C, Back R, Séraphin B, Graille M. 2016. Structure of the active form of Dcp1–Dcp2 decapping enzyme bound to m7GDP and its Edc3 activator. *Nature Structural & Molecular Biology* 23: 982–986.
- Cowieson NP, Aragao D, Clift M, Ericsson DJ, Gee C, Harrop SJ, Mudie N, Panjikar S, Price JR, Riboldi-Tunnicliffe A. 2015. MX1: a bending-magnet crystallography beamline serving both chemical and macromolecular crystallography communities at the Australian Synchrotron. *Journal of Synchrotron Radiation* 22: 187–190.
- Dodds PN, Lawrence GJ, Catanzari AM, Ayliffe MA, Ellis JG. 2004. The *Melampsora lini* AvrL567 avirulence genes are expressed in haustoria and their products are recognized inside plant cells. *Plant Cell* 16: 755–768.
- Dodds PN, Rathjen JP. 2010. Plant immunity: towards an integrated view of plant–pathogen interactions. *Nature Reviews. Genetics* 11: 539–548.
- Dong S, Wang Y. 2016. Nudix effectors: a common weapon in the arsenal of plant pathogens. *PLoS Pathogens* 12: e1005704.
- Dong S, Yin W, Kong G, Yang X, Qutob D, Chen Q, Kale SD, Sui Y, Zhang Z, Dou D *et al.* 2011. *Phytophthora sojae* avirulence effector Avr3b is a secreted NADH and ADP-ribose pyrophosphorylase that modulates plant immunity. *PLoS Pathogens* 7: e1002353.
- Earley KW, Haag JR, Pontes O, Opper K, Juehne T, Song K, Pikaard CS. 2006. Gateway-compatible vectors for plant functional genomics and proteomics. *The Plant Journal* 45: 616–629.
- Evans PR, Murshudov GN. 2013. How good are my data and what is the resolution? *Acta crystallographica Section D, Biological Crystallography* 69: 1204–1214.
- Fonseca JP, Dong X. 2014. Functional characterization of a Nudix hydrolase AtNUDX8 upon pathogen attack indicates a positive role in plant immune responses. *PLoS ONE* 9: e114119.
- Fujimura T, Esteban R. 2010. Yeast double-stranded RNA virus LA deliberately synthesizes RNA transcripts with 5'-diphosphate. *The Journal of Biological Chemistry* 285: 22911–22918.
- Gabelli SB, Bianchet MA, Bessman MJ, Amzel LM. 2001. The structure of ADP-ribose pyrophosphatase reveals the structural basis for the versatility of the Nudix family. *Nature Structural Biology* 8: 467–472.
- Gabelli SB, Bianchet MA, Ohnishi Y, Ichikawa Y, Bessman MJ, Amzel LM. 2002. Mechanism of the *Escherichia coli* ADP-ribose pyrophosphatase, a Nudix hydrolase. *Biochemistry* 41: 9279–9285.
- Ge X, Li G-J, Wang S-B, Zhu H, Zhu T, Wang X, Xia Y. 2007. AtNUDT7, a negative regulator of basal immunity in *Arabidopsis*, modulates two distinct defense response pathways and is involved in maintaining redox homeostasis. *Plant Physiology* 145: 204–215.
- Gloggnitzer J, Akimcheva S, Srinivasan A, Kusenda B, Riehs N, Stampf H, Bautor J, Dekrout B, Jonak C, Jiménez-Gómez JM *et al.* 2014. Nonsense-mediated mRNA decay modulates immune receptor levels to regulate plant antibacterial defense. *Cell Host & Microbe* 16: 376–390.
- Grudzien-Nogalska E, Kiledjian M. 2017. New insights into decapping enzymes and selective mRNA decay. *Wiley Interdisciplinary Reviews. RNA* 8: e1379.
- Gunawardana D, Cheng H-C, Gayler KR. 2008. Identification of functional domains in *Arabidopsis thaliana* mRNA decapping enzyme (AtDcp2). *Nucleic Acids Research* 36: 203–216.
- He F, Celik A, Wu C, Jacobson A. 2018. General decapping activators target different subsets of inefficiently translated mRNAs. *eLife* 7: e34409.
- He F, Wu C, Jacobson A. 2022. Dcp2 C-terminal cis-binding elements control selective targeting of the decapping enzyme by forming distinct decapping complexes. *eLife* 11: e74410.
- Heese A, Hann DR, Gimenez-Ibanez S, Jones AME, He K, Li J, Schroeder JI, Peck SC, Rathjen JP. 2007. The receptor-like kinase SERK3/BAK1 is a central regulator of innate immunity in plants. *Proceedings of the National Academy of Sciences, USA* 104: 12217–12222.
- Höfer K, Li S, Abele F, Frindert J, Schlotthauer J, Grawenhoff J, Du J, Patel DJ, Jäschke A. 2016. Structure and function of the bacterial decapping enzyme NudC. *Nature Chemical Biology* 12: 730–734.
- Ishikawa K, Yoshimura K, Harada K, Fukusaki E, Ogawa T, Tamoi M, Shigeoka S. 2010. AtNUDX6, an ADP-ribose/NADH pyrophosphohydrolase in *Arabidopsis*, positively regulates NPR1-dependent salicylic acid signaling. *Plant Physiology* 152: 2000–2012.
- Islam MR, Mayo GME. 1990. A compendium on host genes in flax conferring resistance to flax rust. *Plant Breeding* 104: 89–100.
- Ito R, Hayakawa H, Sekiguchi M, Ishibashi T. 2005. Multiple enzyme activities of *Escherichia coli* MutT protein for sanitization of DNA and RNA precursor pools. *Biochemistry* 44: 6670–6674.
- Iwai T, Kuramitsu S, Masui R. 2004. The Nudix hydrolase Ndx1 from *Thermus thermophilus* HB8 is a diadenosine hexaphosphate hydrolase with a novel activity. *The Journal of Biological Chemistry* 279: 21732–21739.
- Jemth A-S, Gustafsson R, Bräutigam L, Henriksson L, Vallin KSA, Sarno A, Almlöf I, Homan E, Rasti A, Warpman Berglund U *et al.* 2018. MutT homologue 1 (MTH1) catalyzes the hydrolysis of mutagenic O6-methyl-dGTP. *Nucleic Acids Research* 46: 10888–10904.
- Jones JDG, Dangl JL. 2006. The plant immune system. *Nature* 444: 323–329.
- Jung HW, Panigrahi GK, Jung GY, Lee YJ, Shin KH, Sahoo A, Choi ES, Lee E, Man Kim K, Yang SH *et al.* 2020. Pathogen-associated molecular pattern-triggered immunity involves proteolytic degradation of core nonsense-mediated mRNA decay factors during the early defense response. *Plant Cell* 32: 1081–1101.
- Jurss E, Engel D, Star K, Monson K, Brandt J, Felberg LE, Brookes DH, Wilson L, Chen J, Liles K *et al.* 2018. Improvements to the APBS biomolecular solvation software suite. *Protein Science* 27: 112–128.
- Kabsch W. 2010. XDS. *Acta crystallographica Section D, Biological Crystallography* 66: 125–132.
- Kang L-W, Gabelli SB, Cunningham JE, O'Handley SF, Amzel LM. 2003. Structure and mechanism of MT-ADPase, a Nudix hydrolase from *Mycobacterium tuberculosis*. *Structure* 11: 1015–1023.
- Kong G, Zhao Y, Jing M, Huang J, Yang J, Xia Y, Kong L, Ye W, Xiong Q, Qiao Y *et al.* 2015. The activation of *Phytophthora* effector Avr3b by plant

- cyclophilin is required for the Nudix hydrolase activity of Avr3b. *PLoS Pathogens* 11: e1005139.
- Korneli C, Danisman S, Staiger D. 2014. Differential control of pre-invasive and post-invasive antibacterial defense by the Arabidopsis circadian clock. *Plant & Cell Physiology* 55: 1613–1622.
- Langer G, Cohen SX, Lamzin VS, Perrakis A. 2008. Automated macromolecular model building for X-ray crystallography using ARP/wARP v.7. *Nature Protocols* 3: 1171–1179.
- Lawrence GJ, Anderson PA, Dodds PN, Ellis JG. 2010. Relationships between rust resistance genes at the M locus in flax. *Molecular Plant Pathology* 11: 19–32.
- Leslie NR, McLennan AG, Safrany ST. 2002. Cloning and characterisation of hAps1 and hAps2, human diadenosine polyphosphate-metabolising Nudix hydrolases. *BMC Biochemistry* 3: 20.
- Li Y, Song M, Kiledjian M. 2011. Differential utilization of decapping enzymes in mammalian mRNA decay pathways. *RNA* 17: 419–428.
- Liebschner D, Afonine PV, Baker ML, Bunkóczi G, Chen VB, Croll TI, Hintze B, Hung L-W, Jain S, McCoy AJ. 2019. Macromolecular structure determination using X-rays, neutrons and electrons: recent developments in Phenix. *Acta Crystallographica. Section D, Structural Biology* 75: 861–877.
- Lin J, Abeygunawardana C, Frick DN, Bessman MJ, Mildvan AS. 1996. The role of Glu 57 in the mechanism of the *Escherichia coli* MutT enzyme by mutagenesis and heteronuclear NMR. *Biochemistry* 35: 6715–6726.
- Lin J, Abeygunawardana C, Frick DN, Bessman MJ, Mildvan AS. 1997. Solution structure of the quaternary MutT–M²⁺–AMPCPP–M²⁺ complex and mechanism of its pyrophosphohydrolase action. *Biochemistry* 36: 1199–1211.
- Lo Presti L, Lanver D, Schweizer G, Tanaka S, Liang L, Tollot M, Zuccaro A, Reissmann S, Kahmann R. 2015. Fungal effectors and plant susceptibility. *Annual Review of Plant Biology* 66: 513–545.
- Lu H, McClung CR, Zhang C. 2017. Tick Tock: circadian regulation of plant innate immunity. *Annual Review of Phytopathology* 55: 287–311.
- McLennan AG. 2006. The Nudix hydrolase superfamily. *Cellular and Molecular Life Sciences* 63: 123–143.
- McLennan AG. 2013. Substrate ambiguity among the nudix hydrolases: biologically significant, evolutionary remnant, or both? *Cellular and Molecular Life Sciences* 70: 373–385.
- Mildvan AS, Xia Z, Azurmendi HF, Saraswat V, Legler PM, Massiah MA, Gabelli SB, Bianchet MA, Kang LW, Amzel LM. 2005. Structures and mechanisms of Nudix hydrolases. *Archives of Biochemistry and Biophysics* 433: 129–143.
- Mugridge JS, Ziemniak M, Jemielity J, Gross JD. 2016. Structural basis of mRNA-cap recognition by Dcp1–Dcp2. *Nature Structural & Molecular Biology* 23: 987–994.
- Müller-McNicoll M, Neugebauer KM. 2014. Good cap/bad cap: how the cap-binding complex determines RNA fate. *Nature Structural & Molecular Biology* 21: 9–12.
- Nakamichi N, Kiba T, Kamioka M, Suzuki T, Yamashino T, Higashiyama T, Sakakibara H, Mizuno T. 2012. Transcriptional repressor PRR5 directly regulates clock-output pathways. *Proceedings of the National Academy of Sciences, USA* 109: 17123–17128.
- Nakamichi N, Kita M, Ito S, Sato E, Yamashino T, Mizuno T. 2005. The Arabidopsis pseudo-response regulators, PRR5 and PRR7, coordinately play essential roles for circadian clock function. *Plant & Cell Physiology* 46: 609–619.
- Nguyen VN, Park A, Xu A, Srouji JR, Brenner SE, Kirsch JF. 2016. Substrate specificity characterization for eight putative nudix hydrolases. Evaluation of criteria for substrate identification within the Nudix family. *Proteins* 84: 1810–1822.
- Ogawa T, Ueda Y, Yoshimura K, Shigeoka S. 2005. Comprehensive analysis of cytosolic Nudix hydrolases in *Arabidopsis thaliana*. *The Journal of Biological Chemistry* 280: 25277–25283.
- O'Handley SF, Frick DN, Dunn CA, Bessman MJ. 1998. Orf186 represents a new member of the Nudix hydrolases, active on adenosine (5') triphospho (5') adenosine, ADP-ribose, and NADH. *The Journal of Biological Chemistry* 273: 3192–3197.
- Parrish S, Moss B. 2006. Characterization of a vaccinia virus mutant with a deletion of the D10R gene encoding a putative negative regulator of gene expression. *Journal of Virology* 80: 553–561.
- Parrish S, Moss B. 2007. Characterization of a second vaccinia virus mRNA-decapping enzyme conserved in poxviruses. *Journal of Virology* 81: 12973–12978.
- Parrish S, Resch W, Moss B. 2007. Vaccinia virus D10 protein has mRNA decapping activity, providing a mechanism for control of host and viral gene expression. *Proceedings of the National Academy of Sciences, USA* 104: 2139–2144.
- Perraud A-L, Shen B, Dunn CA, Rippe K, Smith MK, Bessman MJ, Stoddard BL, Scharenberg AM. 2003. NUDT9, a member of the Nudix hydrolase family, is an evolutionarily conserved mitochondrial ADP-ribose pyrophosphatase. *The Journal of Biological Chemistry* 278: 1794–1801.
- Piccirillo C, Khanna R, Kiledjian M. 2003. Functional characterization of the mammalian mRNA decapping enzyme hDcp2. *RNA* 9: 1138–1147.
- Quintas A, Pérez-Núñez D, Sánchez EG, Nogal ML, Hentze MW, Castelló A, Revilla Y. 2017. Characterization of the African swine fever virus decapping enzyme during infection. *Journal of Virology* 91: e00990–17.
- Ravensdale M, Bernoux M, Ve T, Kobe B, Thrall PH, Ellis JG, Dodds PN. 2012. Intramolecular interaction influences binding of the Flax L5 and L6 resistance proteins to their AvrL567 ligands. *PLoS Pathogens* 8: e1003004.
- Rawat R, Takahashi N, Hsu PY, Jones MA, Schwartz J, Salemi MR, Phinney BS, Harmer SL. 2011. REVEILLE8 and PSEUDO-REPONSE REGULATOR5 form a negative feedback loop within the Arabidopsis circadian clock. *PLoS Genetics* 7: e1001350.
- Raxwal VK, Simpson CG, Gloggnitzer J, Entinze JC, Guo W, Zhang R, Brown JWS, Riha K. 2020. Nonsense-mediated RNA decay factor UPF1 is critical for posttranscriptional and translational gene regulation in Arabidopsis. *Plant Cell* 32: 2725–2741.
- Robert X, Gouet P. 2014. Deciphering key features in protein structures with the new ENDscript server. *Nucleic Acids Research* 42: W320–W324.
- Sakumi K, Furuichi M, Tsuzuki T, Kakuma T, Kawabata S, Maki H, Sekiguchi M. 1993. Cloning and expression of cDNA for a human enzyme that hydrolyzes 8-oxo-dGTP, a mutagenic substrate for DNA synthesis. *The Journal of Biological Chemistry* 268: 23524–23530.
- Scarsdale JN, Peculis BA, Wright HT. 2006. Crystal structures of U8 snoRNA decapping Nudix hydrolase, X29, and its metal and cap complexes. *Structure* 14: 331–343.
- Schoenberg DR, Maquat LE. 2012. Regulation of cytoplasmic mRNA decay. *Nature Reviews. Genetics* 13: 246–259.
- Skubák P, Pannu NS. 2013. Automatic protein structure solution from weak X-ray data. *Nature Communications* 4: 2777.
- Song M-G, Bail S, Kiledjian M. 2013. Multiple Nudix family proteins possess mRNA decapping activity. *RNA* 19: 390–399.
- Song M-G, Li Y, Kiledjian M. 2010. Multiple mRNA decapping enzymes in mammalian cells. *Molecular Cell* 40: 423–432.
- Srouji JR, Xu A, Park A, Kirsch JF, Brenner SE. 2017. The evolution of function within the Nudix homology clan. *Proteins* 85: 775–811.
- Stols L, Gu M, Dieckman L, Raffin R, Collart FR, Donnelly MI. 2002. A new vector for high-throughput, ligation-independent cloning encoding a tobacco etch virus protease cleavage site. *Protein Expression and Purification* 25: 8–15.
- Sun Y, Li P, Shen D, Wei Q, He J, Lu Y. 2019. The *Ralstonia solanacearum* effector RipN suppresses plant PAMP-triggered immunity, localizes to the endoplasmic reticulum and nucleus, and alters the NADH/NAD(+) ratio in Arabidopsis. *Molecular Plant Pathology* 20: 533–546.
- Supek F, Bošnjak M, Škunca N, Šmuc T. 2011. REVIGO summarizes and visualizes long lists of gene ontology terms. *PLoS ONE* 6: e21800.
- Tang Q, Liu C, Zhong C, Ding J. 2015. Crystal structures of *Arabidopsis thaliana* Nudix hydrolase NUDT7 reveal a previously unobserved conformation. *Molecular Plant* 8: 1557–1559.
- Terwilliger TC, Grosse-Kunstleve RW, Afonine PV, Moriarty NW, Zwart PH, Hung L-W, Read RJ, Adams PD. 2008. Iterative model building, structure refinement and density modification with the PHENIX AutoBuild wizard. *Acta Crystallographica. Section D, Biological Crystallography* 64: 61–69.
- Trésaugues L, Lundbäck T, Welin M, Flodin S, Nyman T, Silvander C, Gräslund S, Nordlund P. 2015. Structural basis for the specificity of human NUDT16 and its regulation by inosine monophosphate. *PLoS ONE* 10: e0131507.

- Van Dijk E, Cougot N, Meyer S, Babajko S, Wahle E, Séraphin B. 2002. Human Dcp2: a catalytically active mRNA decapping enzyme located in specific cytoplasmic structures. *EMBO Journal* 21: 6915–6924.
- Ve T, Williams SJ, Catanzariti A-M, Rafiqi M, Rahman M, Ellis JG, Hardham AR, Jones DA, Anderson PA, Dodds PN *et al.* 2013. Structures of the flax-rust effector AvrM reveal insights into the molecular basis of plant-cell entry and effector-triggered immunity. *Proceedings of the National Academy of Sciences, USA* 110: 17594–17599.
- Wakamatsu T, Nakagawa N, Kuramitsu S, Masui R. 2008. Structural basis for different substrate specificities of two ADP-ribose pyrophosphatases from *Thermus thermophilus* HB8. *Journal of Bacteriology* 190: 1108–1117.
- Wang W, Barnaby JY, Tada Y, Li H, Tör M, Caldelari D, Lee DU, Fu XD, Dong X. 2011. Timing of plant immune responses by a central circadian regulator. *Nature* 470: 110–114.
- Wang Z, Jiao X, Carr-Schmid A, Kiledjian M. 2002. The hDcp2 protein is a mammalian mRNA decapping enzyme. *Proceedings of the National Academy of Sciences, USA* 99: 12663–12668.
- Waz S, Nakamura T, Hirata K, Koga-Ogawa Y, Chirifu M, Arimori T, Tamada T, Ikemizu S, Nakabeppu Y, Yamagata Y. 2017. Structural and kinetic studies of the human nudix hydrolase MTH1 reveal the mechanism for its broad substrate specificity. *Journal of Biological Chemistry* 292: 2785–2794.
- Westwood ML, O'Donnell AJ, de Bekker C, Lively CM, Zuk M, Reece SE. 2019. The evolutionary ecology of circadian rhythms in infection. *Nature Ecology and Evolution* 3: 552–560.
- Williams CJ, Headd JJ, Moriarty NW, Prisant MG, Videau LL, Deis LN, Verma V, Keedy DA, Hintze BJ, Chen VB *et al.* 2018. MolProbity: more and better reference data for improved all-atom structure validation. *Protein Science* 27: 293–315.
- Wu W, Nemri A, Blackman LM, Catanzariti A-M, Sperschneider J, Lawrence GJ, Dodds PN, Jones DA, Hardham AR. 2019. Flax rust infection transcriptomics reveals a transcriptional profile that may be indicative for rust Avr genes. *PLoS ONE* 14: e0226106.
- Wurm JP, Holdermann I, Overbeck JH, Mayer PH, Sprangers R. 2017. Changes in conformational equilibria regulate the activity of the Dcp2 decapping enzyme. *Proceedings of the National Academy of Sciences, USA* 114: 6034–6039.
- Xu A, Desai AM, Brenner SE, Kirsch JF. 2013. A continuous fluorescence assay for the characterization of Nudix hydrolases. *Analytical Biochemistry* 437: 178–184.
- Xu J, Yang J-Y, Niu Q-W, Chua N-H. 2006. Arabidopsis DCP2, DCP1, and VARICOSE form a decapping complex required for postembryonic development. *Plant Cell* 18: 3386–3398.
- Xu W, Dunn CA, Jones CR, D'Souza G, Bessman MJ. 2004. The 26 Nudix hydrolases of *Bacillus cereus*, a close relative of *Bacillus anthracis*. *The Journal of Biological Chemistry* 279: 24861–24865.
- Yang Q, Huai B, Lu Y, Cai K, Guo J, Zhu X, Kang Z, Guo J. 2020. A stripe rust effector Pst18363 targets and stabilises TaNUDX23 that promotes stripe rust disease. *New Phytologist* 225: 880–895.
- Yoshida S, Ooga T, Nakagawa N, Shibata T, Inoue Y, Yokoyama S, Kuramitsu S, Masui R. 2004. Structural insights into the *Thermus thermophilus* ADP-ribose pyrophosphatase mechanism via crystal structures with the bound substrate and metal. *The Journal of Biological Chemistry* 279: 37163–37174.
- Yu D, Song W, Tan EYJ, Liu L, Cao Y, Jirsitzka J, Li E, Logemann E, Xu C, Huang S *et al.* 2022. TIR domains of plant immune receptors are 2',3'-cAMP/cGMP synthetases mediating cell death. *Cell* 185: 2370–2386.
- Yu X, Li B, Jang G-J, Jiang S, Jiang D, Jang J-C, Wu S-H, Shan L, He P. 2019. Orchestration of processing body dynamics and mRNA decay in Arabidopsis immunity. *Cell Reports* 28: 2194–2205.
- Zha M, Zhong C, Peng Y, Hu H, Ding J. 2006. Crystal structures of human NUDT5 reveal insights into the structural basis of the substrate specificity. *Journal of Molecular Biology* 364: 1021–1033.

Supporting Information

Additional Supporting Information may be found online in the Supporting Information section at the end of the article.

Fig. S1 Structural features of AvrM14.

Fig. S2 Western blots demonstrating the expression and accumulation of the AvrM14 wild-type (WT) and mutant proteins in agroinfiltrated plant tissue.

Fig. S3 Mutation of Nudix-box glutamate E82 to glutamine does not alter the recognition of AvrM14-A or AvrM14-B by M1 when co-expressed in tobacco.

Fig. S4 Recombinant AvrM14 proteins elute as two distinct peaks during size-exclusion chromatography (SEC); all AvrM14 crystal structures display similar self-association interfaces.

Fig. S5 AvrM14-B crystal packing dimer (A, purple) compared with homodimeric *Homo sapiens* Nudt16 (PDB ID: 3MGM) (B, gold) with the Nudix helices coloured green.

Fig. S6 Screening of common Nudix hydrolase substrates using monomeric and homodimeric AvrM14 protein.

Fig. S7 Migration and Rf values for standard solutions of potential mRNA-decapping products.

Fig. S8 Identifying stable multimeric AvrM14 protein complexes from *Nicotiana benthamiana* protein extracts.

Fig. S9 Size-exclusion chromatograms displaying the elution profile of each of the AvrM14 homologues assessed in our study.

Fig. S10 Average expression level (\pm SD) in transcripts per million for AvrM14 genes in each of the RNA-sequencing datasets.

Fig. S11 Co-expression of AvrM14 wild-type and mutant proteins with M1 in tobacco.

Fig. S12 Expression of wild-type and mutant AvrM14 proteins in M1 and M4 flax.

Methods S1 Extended Materials and Methods.

Table S1 DNA and protein sequences used in this study.

Table S2 Crystallography data collection and structure refinement statistics.

Table S3 Substrates and secondary enzymes used in the phosphate sensing fluorophore-based hydrolysis assays with recombinant AvrM14-A.

Table S4 Average read counts with standard deviations in TPM as determined by Salmon, the differential expression (DE) analysis output (\log_2 fc and q -values) as determined by fishpond when comparing the AvrM14-A and vector-only datasets and the BLAST-2-Go best hit for all transcripts.

Table S5 Average read counts with standard deviations in TPM as determined by Salmon, the differential expression (DE) analysis output (\log_2 fc and q -values) as determined by fishpond when comparing the AvrM14-A and AvrM14-AE82Q datasets, and the BLAST-25GO best hit for all transcripts.

Table S6 Summary of the cell-death results recorded during this study following the expression of various AvrM14 proteins in M1 flax, M4 flax and tobacco co-expressing M1.

Please note: Wiley is not responsible for the content or functionality of any Supporting Information supplied by the authors. Any queries (other than missing material) should be directed to the *New Phytologist* Central Office.